


## RESEARCH ARTICLE

# Surface AMP deaminase 2 as a novel regulator modifying extracellular adenine nucleotide metabolism

Lisa Ehlers<sup>1,2</sup>  | Aditi Kuppe<sup>1,2</sup> | Alexandra Damerau<sup>1,2</sup> | Siska Wilantri<sup>1,2</sup> | Marieluise Kirchner<sup>3</sup> | Philipp Mertins<sup>3</sup> | Cindy Strehl<sup>1,2</sup> | Frank Buttgereit<sup>1,2</sup> | Timo Gaber<sup>1,2</sup>

<sup>1</sup>Department of Rheumatology and Clinical Immunology, Charité-Universitätsmedizin Berlin, Corporate Member of Freie Universität Berlin, Humboldt-Universität zu Berlin, Berlin, Germany

<sup>2</sup>Deutsches Rheuma-Forschungszentrum (DRFZ) Institute of the Leibniz Association, Berlin, Germany

<sup>3</sup>BIH Core Unit Proteomics, Berlin Institute of Health (BIH) and Max-Delbrück-Centrum für Molekulare Medizin (MDC), Berlin, Germany

## Correspondence

Lisa Ehlers, Department of Rheumatology and Clinical Immunology, Charité-Universitätsmedizin Berlin, Corporate Member of Freie Universität Berlin, Humboldt-Universität zu Berlin, Berlin Institute of Health (BIH), Charitéplatz 1, 10117 Berlin, Germany.  
Email: lisa.ehlers@charite.de

## Funding information

Horizon Pharma, Grant/Award Number: 112517; Studienstiftung des Deutschen Volkes (Studienstiftung); Alexandra Damerau; Deutsche Forschungsgemeinschaft (DFG), Grant/Award Number: 353142848

## Abstract

Adenine nucleotides represent crucial immunomodulators in the extracellular environment. The ectonucleotidases CD39 and CD73 are responsible for the sequential catabolism of ATP to adenosine via AMP, thus promoting an anti-inflammatory milieu induced by the “adenosine halo”. AMPD2 intracellularly mediates AMP deamination to IMP, thereby both enhancing the degradation of inflammatory ATP and reducing the formation of anti-inflammatory adenosine. Here, we show that this enzyme is expressed on the surface of human immune cells and its predominance may modify inflammatory states by altering the extracellular milieu. Surface AMPD2 (eAMPD2) expression on monocytes was verified by immunoblot, surface biotinylation, mass spectrometry, and immunofluorescence microscopy. Flow cytometry revealed enhanced monocytic eAMPD2 expression after TLR stimulation. PBMCs from patients with rheumatoid arthritis displayed significantly higher levels of eAMPD2 expression compared with healthy controls. Furthermore, the product of AMPD2—IMP—exerted anti-inflammatory effects, while the levels of extracellular adenosine were not impaired by an increased eAMPD2 expression. In summary, our study identifies eAMPD2 as a novel regulator of the extracellular ATP-adenosine balance adding to the immunomodulatory CD39-CD73 system.

## KEYWORDS

adenosine, inflammation, nucleotidases, purines, rheumatoid arthritis, RRIDs

**Abbreviations:** A1R, adenosine A1 receptor; A2AR, adenosine A2A receptor; A2BR, adenosine A2B receptor; A3R, adenosine A3 receptor; AMPD2, AMP deaminase 2; BFA, brefeldin A; BL, B lymphocyte; DC, dendritic cell; Dex, dexamethasone; eADO, extracellular adenosine; eAMPD2, surface AMP deaminase 2; eATP, extracellular ATP; FDR, false discovery rate; iBAQ, intensity-based absolute quantification; IP, immunoprecipitation; LFQ, label-free quantification; MN, monensin; MSC, mesenchymal stromal cell; MTX, methotrexate; PBMC, peripheral blood mononuclear cell; scr, scrambled; T<sub>H</sub> cell, T helper cell; TLR, Toll-like receptor; Treg, regulatory T cell.

This is an open access article under the terms of the Creative Commons Attribution-NonCommercial-NoDerivs License, which permits use and distribution in any medium, provided the original work is properly cited, the use is non-commercial and no modifications or adaptations are made.

© 2021 The Authors. The FASEB Journal published by Wiley Periodicals LLC on behalf of Federation of American Societies for Experimental Biology.

# 1 | INTRODUCTION

In recent years, extracellular adenosine (eADO) has emerged as an important factor in the pathogenesis of immune-mediated and neoplastic diseases.<sup>1,2</sup> eADO is mainly provided by the degradation of extracellular ATP (eATP) through the subsequent action of different ectonucleotidases.<sup>3</sup> The process of enzymatic ADO production is subdivided into two interacting pathways: the more prominent canonical pathway and the alternative pathway. The canonical pathway consists of the rate-limiting ectonucleoside triphosphate diphosphohydrolase-1 (CD39) and the ecto-5'-nucleotidase (CD73). While CD39 catalyzes the dephosphorylation of ATP and ADP to AMP, CD73 mediates the phosphorolytic cleavage of the latter, thereby producing ADO.<sup>4</sup> On the other hand, the alternative pathway involves the conversion of extracellular NAD<sup>+</sup> to ADP ribose by CD38, followed by AMP production by CD203a/PC-1.<sup>5,6</sup> These pathways of ADO generation are completed by an additional ectoenzyme—adenosine deaminase—that terminates ADO action by deamination to inosine.<sup>7</sup> Beyond ectoenzyme activity, extracellular adenine nucleotide levels are determined by cellular uptake and release via channel proteins and nucleoside transporters.<sup>8-11</sup>

Extracellular purine metabolites signal via two major classes of receptors: P2 receptors mediate the action of purine nucleotides like ATP. The P1 receptor family, on the other hand, consists of four ADO receptors (A1R, A2AR, A2BR, A3R) that signal via different G-proteins.<sup>12</sup> Purinergic receptors are expressed ubiquitously throughout different tissues and elicit a myriad of effects.<sup>13</sup> Our work focuses on the role of adenine nucleotides in the context of inflammation.

The increasing understanding of the regulation of eADO production as well purinergic signaling has enhanced the development of therapeutic concepts involving adenosinergic pathways.<sup>1,12,14,15</sup> eATP is released from cells under conditions of stress and inflammation, thereby functioning as an alarm in provoking a pro-inflammatory reaction.<sup>16-23</sup> In contrast, eADO represents a potent anti-inflammatory agent.<sup>24-33</sup> Anti-inflammatory effects of eADO have mainly been attributed to the activation of A2R and A3R and agonists of these receptors are currently being evaluated as therapeutic agents to treat inflammatory conditions.<sup>34-38</sup>

Besides ADO receptors, leukocytes are also equipped with ectonucleotidases permitting a regulation of the inflammatory environment by both ATP breakdown and ADO generation. CD39 and CD73 are differentially expressed on distinct immune cell subsets. While CD39 expression is present in the majority of neutrophils, dendritic cells (DC), monocytes and B lymphocytes (BL) as well as a subset of regulatory T cells (Treg), CD73 is expressed by DCs, BLs, cytotoxic T cells, and several non-immune cells like mesenchymal stromal cells (MSC) and endothelial cells.<sup>39-46</sup> In contrast, only a small subset of CD4<sup>+</sup> T helper (T<sub>H</sub>) cells is characterized by CD39 or CD73

expression.<sup>47</sup> Recent research has revealed a dysregulation of the adenosinergic system in many autoimmune diseases.<sup>48-51</sup>

Conversely, enhanced tumor growth has been ascribed to a surplus of anti-inflammatory eADO.<sup>52-55</sup> Therefore, blocking eADO generation or ADO receptor signaling might eliminate the protective “adenosine halo” and restore an environment permitting an effective anti-tumor immune response.<sup>2,12,56</sup> Recent approaches examining this therapeutic concept have yielded promising results.<sup>57-61</sup> These findings demonstrate the clinical relevance of adenosinergic signaling and highlight the importance of a deep understanding of extracellular purine metabolism.

In this context, we noticed that the ensemble of ectoenzymes implicated in the regulation of extracellular adenine nucleotides is incomplete compared with the complex network of reactions involved in intracellular purine metabolism.<sup>62</sup> While AMP deamination substantially modifies cytosolic purine content, it has hitherto not been recognized as an essential reaction in the extracellular space. Although previous studies have reported attachment of AMP deaminases (AMPDs) to the muscle surface and the inner erythrocyte membrane,<sup>63-66</sup> surface expression of AMPD in human leukocytes has not yet been described. AMPDs are responsible for the conversion of AMP to IMP by hydrolyzing the amino group from the 6-position of the adenine nucleotide ring. In contrast to adenine nucleotides, the immunomodulatory role of IMP in the extracellular space remains unclear. AMP deamination facilitates the removal of AMP that accumulates in states of energy depletion. By increasing the ATP:AMP ratio, AMPDs promote energy yield from ATP hydrolysis.<sup>62,67-69</sup> At the same time, AMPDs compete with 5'-nucleotidases for AMP supply, thereby impeding the formation of anti-inflammatory ADO. Conversely, loss of function mutations in the AMPD genes as well as the development of AMPD inhibitors have shown that reduced AMP deamination is associated with an increase in ADO levels.<sup>70-72</sup> We hypothesized that this principle might be equally relevant to the modification of extracellular purine levels under inflammatory conditions. Therefore, we examined AMPD expression on the outer plasma membrane of immune cells.

Here, we demonstrate that AMPD2 is expressed on the cell surface of primary human leukocytes and may function as a novel regulator of extracellular purine metabolism, thereby modifying the ATP-adenosine balance controlled by the CD39-CD73 ectonucleotidase system (Figure 1).

## 2 | MATERIALS AND METHODS

### 2.1 | Subjects

Fifteen patients with a diagnosis of rheumatoid arthritis (RA) were recruited as part of the Charité Rh-GIOP

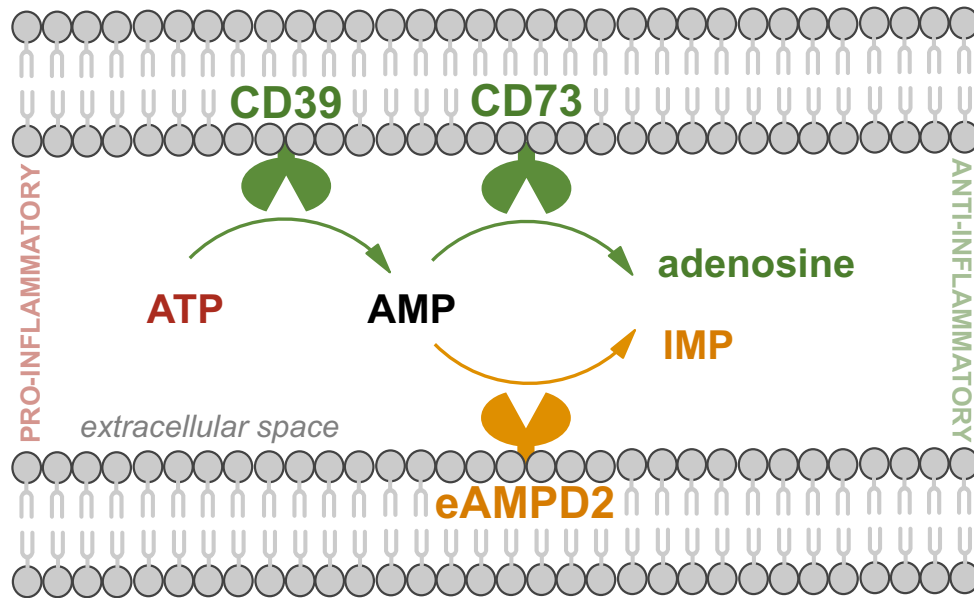


**FIGURE 1** Possible role of eAMPD2 as a novel regulator of extracellular purine metabolism

study at the Department of Rheumatology and Clinical Immunology at Charité-Universitätsmedizin Berlin, Germany. Patients with active disease and in remission were considered for the study. Patients were included irrespective of their current immunosuppressive therapy. Thirteen healthy donors were matched for sex and age. The study was performed in accordance with the Declaration of Helsinki and ethical approval was obtained from the local ethics committee (Charité-Universitätsmedizin Berlin, approval number EA1/207/17). All participants gave informed written consent.

## 2.2 | Preparation of peripheral blood leukocytes and magnetic cell separation

Peripheral venous blood was collected in lithium heparin tubes. Isolation of polymorphonuclear leukocytes was preceded by red blood cell lysis using erythrocyte lysis buffer (0.01 M  $\text{KHCO}_3$ , 0.155 M  $\text{NH}_4\text{Cl}$ , 0.1 mM EDTA, pH 7.5). CD15+ neutrophil granulocytes were purified by magnetic activated cell sorting (MACS) with anti-CD15-microbeads (Miltenyi Biotec, Bergisch Gladbach, Germany, Cat# 130-094-530, RRID:AB\_2814656). Peripheral blood mononuclear cells (PBMCs) were isolated from the blood samples by Ficoll-Paque PLUS (GE Healthcare, Chicago, Illinois) density gradient centrifugation. CD14+ monocytes were isolated from PBMCs by MACS using anti-CD14-microbeads provided by Miltenyi Biotec (Cat# 130-050-201, RRID:AB\_2665482). Cell preparations were performed according to the manufacturer's instructions. Purity of isolated CD14+ monocytes and CD15+ neutrophils exceeded 97% as verified by flow cytometry (Figure S1B+C).

## 2.3 | Chemicals and reagents

Dulbecco's Modified Eagle Medium (DMEM), Roswell Park Memorial Institute 1640 Medium (RPMI), MCDB 131 Medium, penicillin, streptomycin, and L-glutamine were obtained from Gibco (Thermo Fisher Scientific, Waltham, Massachusetts). Fetal calf serum (FCS), human AB serum,  $\beta$ -mercaptoethanol (2-ME), Accutase solution, brefeldin A (BFA), monensin (MN), lipopolysaccharide (LPS), flagellin (FltC), phytohemagglutinin-L (PHA-L), Phorbol 12-myristate 13-acetate (PMA), ionomycin, dexamethasone (Dex), hydrocortisone, Epidermal Growth Factor (EGF), ATP, ADO, IMP, and inosine were purchased from Sigma-Aldrich (St. Louis, Missouri). Miltenyi Biotec provided Poly (I:C) and ODN 2006. Pam3CSK4, FSL-1, and Resiquimod (R848) were purchased from Tocris (Bristol, United Kingdom).

## 2.4 | Antibodies

Staining for flow cytometry was performed using antibodies against AMPD2 (unconjugated, 1:50, rabbit polyclonal, Thermo Fisher Scientific, Cat# PA5-26127, RRID:AB\_2543627), CD3 (Brilliant Violet 510, 1:20, OKT3, BioLegend, San Diego, California, Cat# 317332, RRID:AB\_2561943), CD3 (Alexa Fluor 594, 1:20, UCHT1, DRFZ, Cat# UCHT1, RRID:AB\_2619695), CD4 (APC-Vio 770, 1:10, M-T321, Miltenyi Biotec, Cat# 130-100-357, RRID:AB\_2657994), CD8 (Alexa Fluor 647, 1:200 and Alexa Fluor 700, 1:1600, GN11/134D7, DRFZ), CD14 (FITC, 1:400, TM1, DRFZ), CD14 (Brilliant Violet 650, 1:20, M5E2, BioLegend, Cat# 301835, RRID:AB\_11204241), CD15 (FITC, 1:10, VIMC6, Miltenyi Biotec, Cat# 130-081-101,

RRID:AB\_244217), CD16 (APC/Cyanin7, 1:50, 3G8, BioLegend, Cat# 302018, RRID:AB\_314218), CD19 (PerCP/Cyanine5.5, 1:100, HIB19, BioLegend, Cat# 302230, RRID:AB\_2073119), CD25 (Brilliant Violet 785, 1:20, BC96, BioLegend, Cat# 302637, RRID:AB\_11219197), CD39 (APC, 1:100, REA739, Miltenyi Biotec, Cat# 130-110-789, RRID:AB\_2657891), CD45 (FITC, 1:20, HI30, BioLegend, Cat# 304006, RRID:AB\_314394), CD45RA (Pacific Orange, 1:50, 4G11, DRFZ), CD73 (Brilliant Violet 421, 1:50, AD2, BioLegend, Cat# 344008, RRID:AB\_11204424), CD127 (PE, 1:25, REA614, Miltenyi Biotec, Cat# 130-109-514, RRID:AB\_2654831), CD127 (FITC, 1:10, MB15-18C9, Miltenyi Biotec, Cat# 130-098-093, RRID:AB\_2659850), CCR4 (Brilliant Violet 605, 1:20, L291H4, BioLegend, Cat# 359418, RRID:AB\_2562483), CCR6 (APC, 1:20, REA190, Miltenyi Biotec, Cat# 130-100-373, RRID:AB\_2655933), and CXCR3 (PE-Vio 770, 1:50, REA232, Miltenyi Biotec, Cat# 130-101-382, RRID:AB\_2655739). Goat anti-rabbit IgG (PE, 1:200, Invitrogen, Cat# P2771MP, RRID:AB\_221651), streptavidin (PE, 1:200, Life Technologies, Cat# S866) and streptavidin (APC/Cyanine7, 1:300, BioLegend Cat# 405208) were used as secondary reagents. The following isotype controls were utilized to verify the staining: rabbit IgG (unconjugated, 1:125, Invitrogen, Carlsbad, California, Cat# 02-6102, RRID:AB\_2532938), REA Control (S) (APC, 1:10, Miltenyi Biotec, Cat# 130-113-434, RRID:AB\_2733447), and Mouse IgG1,  $\kappa$  Isotype Ctrl Antibody (Brilliant Violet 421, 1:50, MOPC-21, BioLegend, Cat# 400157, RRID:AB\_10897939). The following antibodies were used for immunofluorescence microscopy: anti-AMPD2 antibody (unconjugated, 1:50, rabbit polyclonal, Thermo Fisher Scientific, Cat# PA5-26127, RRID:AB\_2543627) and goat anti-rabbit IgG (Alexa Fluor Plus 488, 1:500, Thermo Fisher Scientific, Cat# A32731, RRID:AB\_2633280). Antibodies against AMPD2 (1:500, QQ13, SCBT, Dallas, Texas, Cat# sc-100504, RRID:AB\_2258261), beta Actin (1:10 000, BA3R, Invitrogen, Cat# MA5-15739, RRID:AB\_10979409), glyceraldehyde 3-phosphate dehydrogenase (GAPDH) (1:100, 6C5, Merck Millipore, Burlington, Massachusetts, Cat# MAB374, RRID:AB\_2107445), alpha Tubulin (100 ng/mL, rabbit polyclonal, abcam, Cambridge, United Kingdom, Cat# ab4074, RRID:AB\_2288001), pan Cadherin (1:500, CH-19, abcam, Cat# ab6528, RRID:AB\_305544), CD14 (Biotin, 1:50, TM1, DRFZ), lamin B1 (1:200, B-10, SCBT, Cat# sc-374015, RRID:AB\_10947408), cytochrome b (1:200, SCBT, Cat# sc-11436, RRID:AB\_2088887), calreticulin (1:2000, Thermo Fisher Scientific, Cat# PA1-902A, RRID:AB\_2069607), mouse IgG (HRP, 1:10 000, Promega, Madison, Wisconsin, Cat# W4021, RRID:AB\_430834), rabbit IgG (HRP, 1:10 000, Promega, Cat# W4011, RRID:AB\_430833), chicken IgY (HRP, 1:5000, Thermo Fisher Scientific Cat# A16054, RRID:AB\_2534727) and streptavidin (HRP, 1:1000, R&D Systems, Minneapolis,

Minnesota, Cat# DY998) were used for western blot analysis. Mouse monoclonal (2  $\mu$ L, QQ13, SCBT, Cat# sc-100504, RRID:AB\_2258261) and rabbit polyclonal (3  $\mu$ L, Thermo Fisher Scientific, Cat# PA5-26127, RRID:AB\_2543627) anti-AMPD2 antibodies were applied to realize immunoprecipitation (IP) of AMPD2, while mouse IgG1 (1:10, 2  $\mu$ L, Invitrogen, Cat# 02-6100, RRID:AB\_2532935) and rabbit IgG (1,2  $\mu$ L, Invitrogen, Cat# 02-6102, RRID:AB\_2532938) served as isotype controls.

## 2.5 | Cell culture

Human embryonic kidney 293 (HEK293) cells (Cat# CRL-1573, RRID:CVCL\_0045) were purchased from ATCC (Manassas, Virginia) and cultured in DMEM supplemented with 10% (v/v) FCS. Jurkat (ATCC, Cat# TIB-152, RRID:CVCL\_0367), THP-1 (ATCC, Cat# TIB-202, RRID:CVCL\_0006) and U-937 (ATCC, Cat# CRL-1593, RRID:CVCL\_0007) cells were cultured in RPMI supplemented with 10% (v/v) FCS. Human microvascular endothelial cells-1 (HMEC-1) (ATCC, Cat# CRL-10636, RRID:CVCL\_0307) were cultured in MCDB 131 Medium supplemented with 25% (v/v) FCS, 2 mM L-glutamine, 10 ng/mL EGF and 0.3  $\mu$ g/mL hydrocortisone. Human primary immune cells were cultured in RPMI supplemented with 10% (v/v) human AB serum. 100 U/mL penicillin, 100  $\mu$ g/mL streptomycin and 50  $\mu$ M 2-ME were added to all media used. Cells were incubated in a humidified atmosphere at 5% CO<sub>2</sub> and approximately 18% O<sub>2</sub>. Hypoxia was established by placing the cells in a hypoxic chamber (Binder) at 1% O<sub>2</sub>. Incubation with either 1  $\mu$ g/mL Pam3CSK4, 10  $\mu$ g/mL Poly (I:C), 1  $\mu$ g/mL LPS, 100 ng/mL FliC, 1  $\mu$ g/mL FSL-1, 1  $\mu$ g/mL R848, 0.5  $\mu$ M ODN 2006, 5  $\mu$ g/mL PHA-L, or 10 ng/mL PMA and 1  $\mu$ g/mL ionomycin was performed as indicated to provoke immunostimulation. Inhibition of the golgi apparatus was achieved by incubation with 1  $\mu$ g/mL BFA or 0.5  $\mu$ g/mL MN. Dex was applied at concentrations of 10<sup>-5</sup> M or 10<sup>-8</sup> M as indicated while methotrexate (MTX) (medac, Wedel, Germany) was utilized at 0.8  $\mu$ M. Adherent cells were detached with the help of Accutase solution for 5 minutes at 37°C.

## 2.6 | Transfection of HEK293 cells with short hairpin RNA (shRNA)

Bacterial stocks containing shRNA plasmids cloned into the pLKO.1 puro vector were purchased from Sigma-Aldrich (MISSION shRNA). Hairpin sequences are provided in Table 1. The empty lentiviral backbone of pLKO.1 puro was provided by Bob Weinberg (Addgene plasmid #8453; <http://n2t.net/addgene:8453>; RRID:Addgene\_8453)

**TABLE 1** shRNA sequences targeting AMPD2

sh1	CCGGCCAAGGCCAAATATCCCTTTACTCGAGTAAAGGGATATTTGGCCTTGGTTTTTG
sh2	CCGGGCGCTTCATCAAGCGGGCAATCTCGAGATTGCCCGCTTGATGAAGCGCTTTTTG
sh3	CCGGGGGTATCTGGGAAGTACTTTGCTCGAGCAAAGTACTTCCCAGATACCCTTTTTTG
sh4	CCGGCATCGCTTTGACAAGTTAATCTCGAGATTAACTTGTCAAAGCGATGTTTTTG
sh5	CCGGGCACGTCTATGGATGGCAAATCTCGAGATTGCCATCCATAGACGTGCTTTTTG
sh6	CCGGATGTGCTGGAACGGGAGTTTCTCGAGGAACTCCCGTCCAGCACATTTTTTTG
sh7	CCGGGCCTCTTTGATGTGTACCGTACTCGAGTACGGTACACATCAAAGAGGCTTTTTG
sh8	CCGGTCATGCTGGCTGAGAACATTTCTCGAGAAATGTTCTCAGCCAGCATGATTTTTTG

whereas the plasmid containing scrambled shRNA was a gift from David Sabatini (Addgene plasmid #1864; <http://n2t.net/addgene:1864>; RRID:Addgene\_1864).<sup>73,74</sup> Bacterial colonies were cultured according to the manufacturer's instructions and plasmid DNA was prepared using NucleoBond Xtra EF (Macherey-Nagel, Düren, Germany). HEK293 cells were transfected with 30 µg of each plasmid to achieve transient knockdown of AMPD2.

## 2.7 | Lentivirus production and transduction of HEK293 and U-937 cells

Viral particles were produced by co-transfecting HEK293 cells with packaging plasmids pPAX2 and pVSVG by means of calcium phosphate precipitation. Viral supernatants were harvested after 48 hours and supplemented with 10 µg/mL polybrene (Sigma-Aldrich). Infection of HEK293 and U-937 cells was achieved by centrifugation for 2 hours at 700 g and 32°C. Successfully transduced cells were selected for at least 10 days by adding 1 µg/mL puromycin (InvivoGen, San Diego, California) to the culture medium.

## 2.8 | Sample preparation for protein analysis

Whole cell protein was prepared by lysing 10<sup>6</sup> cells in 20 µL Laemmli sample buffer (Bio-Rad, Hercules, California, Cat# 1610747). IP lysis buffer (10 mM Tris HCl pH 7.5, 10 mM NaCl, 2 mM EDTA, 0.1% (v/v) Triton X-100, 1 mM PMSF, 2 µg/mL aprotinin) supplemented with protease and phosphatase inhibitor (Thermo Fisher Scientific, Cat# 78440) yielded whole cell lysates suitable for IP: 10 × 10<sup>6</sup> cells were lysed in 300 µL IP lysis buffer for 5 minutes on ice. 12 µL 3 M NaCl were added for another 10 minutes prior to centrifugation for 15 minutes at 16 000 g and 4°C, yielding a clear supernatant. Cytosolic and membrane fractions were prepared using the Mem-PER Plus Membrane Protein Extraction Kit (Thermo Fisher Scientific, Cat# 89842). Additionally, surface protein enriched samples were obtained

by surface biotinylation followed by streptavidin-based pull-down (Pierce Cell Surface Protein Isolation Kit, Thermo Fisher Scientific). The manufacturer's protocols were followed for both procedures. In order to concentrate cytosolic and membrane fractions prior to sodium dodecyl sulfate polyacrylamide gel electrophoresis (SDS-PAGE), the lysates were concentrated using Amicon Ultra-0.5 mL Centrifugal Filters (50K, Merck Millipore Ltd., Ireland). Prior to IP or SDS-PAGE, respectively, protein concentrations of the lysates were determined by bicinchoninic acid assay (BCA assay, Interchim, Montluçon, France) and equal protein amounts were applied to the subsequent procedure. Before IP, the lysates were precleared with 20 µL protein A/G plus agarose (SCBT, Cat# sc-2003, RRID:AB\_10201400) for 30 minutes at 4°C. IP of AMPD2 was performed by incubating 1 mL lysate with either antibody against AMPD2 or isotype control overnight. Pull-down was achieved by adding 20 µL protein A/G plus agarose and four 5-minute washing steps with 1 mL IP buffer (0.15 M NaCl, 0.05 M Tris-HCl pH 8, 1% (v/v) NP40) supplemented with protease and phosphatase inhibitor (Thermo Fisher Scientific, Cat# 78440) followed by centrifugation at 1000 g for one minute. Agarose pellets were prepared for SDS-PAGE by adding 6.5 µL 4× Laemmli sample buffer (Bio-Rad, Cat# 1610747) or directly digested for mass spectrometric analysis (see *Protein Digest* below).

## 2.9 | Western blot analysis

Samples were separated by SDS-PAGE and subsequently blotted onto PVDF membranes (Merck Millipore). PVDF membranes were block with 5% (w/v) nonfat dry milk (AppliChem GmbH, Darmstadt, Germany) in TBS/0.05% Tween 20 (Sigma-Aldrich) for 90 minutes followed by three 10-minute washing steps with TBS/0.05% Tween 20. Protein detection was accomplished with the aforementioned antibodies diluted in TBS/0.05% Tween 20: the membranes were incubated with the primary antibody for 2 hours at room temperature (RT) or overnight at 4°C. The secondary antibody was added for 1 hour at RT. Each step was followed by three 10-minute washing steps with TBS/0.05% Tween

20. Visualization was accomplished by enzymatic chemiluminescence (PerkinElmer, GE Healthcare) in an ImageQuant LAS 4000 imager (GE Healthcare).

## 2.10 | Protein digest

Antibody pull-down samples were processed for mass spectrometry as follows: Dry beads were resuspended in 20  $\mu$ L urea buffer (6 M urea, 2 M thiourea, 10 mM HEPES, pH 8.0) and reduced for 30 minutes at RT in 12 mM dithiothreitol solution, followed by alkylation by 40 mM chloroacetamide for 20 minutes in the dark at RT. The samples were first digested using 1  $\mu$ g endopeptidase LysC (Wako, Osaka, Japan) for 4 hours, followed by dilution in 4 volumes of 50 mM ammonium bicarbonate buffer (pH = 8.5) and digestion with 1  $\mu$ g sequence-grade trypsin (Promega) for 16h. The digestion was stopped by acidifying each sample to pH < 2.5 by adding trifluoroacetic acid solution (final concentration 1%). The peptides were extracted and desalted using the StageTip protocol.<sup>75</sup> Samples from streptavidin pull-down experiments were processed using the SP3 protein clean-up and digestion protocol.<sup>76</sup> Peptides were collected, extracted, and desalted using the StageTip protocol.<sup>75</sup> Proteins from total cell lysate, cytosolic and membrane fraction (input samples) were extracted with 6 M Guanidinium chloride/50 mM ammonium bicarbonate buffer (pH = 8.5) and reduced for 30 minutes at RT in 12 mM dithiothreitol solution, followed by alkylation by 40 mM chloroacetamide for 20 minutes in the dark at RT. The samples were digested and desalted as described above.

## 2.11 | LC-MS/MS analyses

For LC-MS/MS analyses peptides were eluted with 80% Acetonitrile/0.1% formic acid, dried and resolved in 3% acetonitrile/0.1% formic acid. Peptides were separated on a reversed-phase column (20 cm fritless silica microcolumns with an inner diameter of 75  $\mu$ m, packed with ReproSil-Pur C18-AQ 1.9  $\mu$ m resin (Dr Maisch GmbH, Ammerbuch-Entringen, Germany)) with a 250 nL/min flow rate of increasing Buffer B concentration (from 2% to 60%) on a High Performance Liquid Chromatography (HPLC) system (Thermo Fisher Scientific). A 90-minute gradient was applied for antibody-based and streptavidin-based pull-down samples, whereas a 202-minute gradient was applied for input samples. Peptides from pull-down samples were analyzed on a Q Exactive Plus or HF-X Hybrid Quadrupole-Orbitrap instrument (Thermo Fisher Scientific). Input sample measurements were performed with an Orbitrap Fusion Tribrid instrument (Thermo Fisher Scientific). The Q Exactive Plus instrument was run in data dependent mode selecting the Top 10 most intense ions in the MS full scans, selecting ions from

350 to 2000  $m/z$ , using 70K resolution with a  $3 \times 10^6$  ion count target and 50 ms injection time. Tandem MS was performed by isolation at 1.6  $m/z$  with the quadrupole, HCD fragmentation with normalized collision energy of 26 and resolution of 17.5K. The MS<sup>2</sup> ion count target was set to  $5 \times 10^4$  with a maximum injection time of 250 ms For measurements with the HF-X instrument the Top 20 most intense ions in the MS full scans from 350 to 1800  $m/z$  were selected, using 60K resolution with a  $3 \times 10^6$  ion count target and 10 ms injection time. Tandem MS was performed by isolation at 1.3  $m/z$  with the quadrupole, HCD fragmentation with normalized collision energy of 27 and resolution of 15K. The MS<sup>2</sup> ion count target was set to  $1 \times 10^5$  with a maximum injection time of 22 ms The Orbitrap Fusion Tribrid instrument was run in data dependent mode selecting the top 20 most intense ions in the MS full scans, selecting ions from 350 to 2000  $m/z$ , using 60K resolution with a  $4 \times 10^5$  ion count target and 50 ms injection time. Tandem MS was performed by isolation at 0.7  $m/z$  with the quadrupole, HCD fragmentation with normalized collision energy of 32 and resolution of 15K. The MS<sup>2</sup> ion count target was set to  $5 \times 10^4$  with a maximum injection time of 250 ms For all measurements only precursors with charge state 2-7 were sampled for MS<sup>2</sup>. The dynamic exclusion duration was set to 30 seconds with a 10 ppm tolerance around the selected precursor and its isotopes. Data were analyzed using the MaxQuant software package (v1.6.0.1). The internal Andromeda search engine was used to search MS<sup>2</sup> spectra against a decoy human UniProt database (HUMAN.2017, HUMAN.2019) containing forward and reverse sequences. The search included variable modifications of methionine oxidation and N-terminal acetylation, deamidation (N and Q) and fixed modification of carbamidomethyl cysteine. Minimal peptide length was set to seven amino acids and a maximum of 3 missed cleavages was allowed. The FDR (false discovery rate) was set to 1% for peptide and protein identifications. Unique and razor peptides were considered for quantification. Retention times were recalibrated based on the built-in nonlinear time-rescaling algorithm. MS<sup>2</sup> identifications for technical replicates were transferred between runs with the "Match between runs" option. iBAQ values and LFQ (label-free quantification) intensities were calculated using the in-built algorithms. The resulting text files were filtered to exclude reverse database hits, potential contaminants, and proteins only identified by site. The mass spectrometry proteomics data have been deposited to the ProteomeXchange Consortium via the PRIDE partner repository with the dataset identifier PXD022350.<sup>77</sup>

## 2.12 | Flow cytometry

Staining for flow cytometry was performed on ice. Dead cell removal (Miltenyi Biotec) was performed prior to

the staining as indicated. The cells were resuspended in PBS/0.5% BSA/0.05% sodium azide (PBA). 10% (v/v) human IgG (Kiovig [100 mg/mL, 1:2 dilution], Baxter AG, Wien, Austria) was added to block unspecific binding of Fc receptors. Specificity was ensured by incubating the cells with 25-fold excess unconjugated antibody for 10 minutes prior to the staining procedure to block binding of the primary antibody. Cells were incubated with a combination of the aforementioned antibodies for 10 minutes followed by two 3-minute washing steps with PBA at 300 g and 4°C. Where applicable, cells were subsequently incubated with a secondary antibody for 10 minutes and washed as before. Apoptotic cells were identified using annexin V (Cy5, 1:100, BD, Franklin Lakes, New Jersey, Cat# 559934, RRID:AB\_2869267), while 7-AAD (1:100, BD, Cat# 559925, RRID:AB\_2869266) and DAPI (1 µg/mL, Sigma-Aldrich) were applied to exclude dead cells. Cells were fixed and permeabilized with -20°C cold 90% (v/v) methanol to complete intracellular stainings. The samples were measured using a MACSQuant Analyzer 10 (Miltenyi Biotec) and an LSRFortessa cell analyzer (BD) and analyzed with FlowJo software (version 7.6.4 and 10.7.1, BD). eAMPD2, CD39 and CD73 expression was recorded by determining geometric mean fluorescence intensity (gMFI). Results are provided as the ratio (*r* gMFI) of staining to either block or secondary antibody control. Lymphocyte subsets were analyzed as follows: CD4+ T cell subsets were subdivided into Type 1 helper (T<sub>H</sub>1) cells, Type 2 helper (T<sub>H</sub>2) cells and IL-17-producing T helper (T<sub>H</sub>17) cells. T<sub>H</sub>1 cells were identified by the expression of CXCR3 in the absence of CCR4 and CCR6. T<sub>H</sub>2 cells were defined as CCR4+CXCR3-CCR6-, while T<sub>H</sub>17 cells co-expressed CCR4 and CCR6 in the absence of CXCR3. CD4+CD25+CD127low cells were defined as regulatory T cells (Treg).<sup>78</sup> Cytotoxic T cells and B cells were identified by the expression of CD8 and CD19, respectively. Monocytes were subanalyzed according to CD14 and CD16 surface expression as follows: classical (CD14<sup>hi</sup>, CD16-), intermediate (CD14<sup>hi</sup>, CD16+) and non-classical (CD14<sup>low</sup>, CD16<sup>hi</sup>).<sup>79</sup> The gating strategy is depicted in Figure S1A,E.

### 2.13 | Immunofluorescence microscopy

Human PBMCs were seeded onto 8-well chamber slides directly after isolation, while U-937 cells were stained in a 48-well plate and subsequently centrifuged onto a glass slide at 500 g for 1 minute with the help of a Cytospin 4 cytocentrifuge (Thermo Fisher Scientific). The cells were fixed with 4% paraformaldehyde for 8 minutes followed by three 3-minute washing steps with PBS. In order to achieve intracellular staining the cells were permeabilized prior to the staining procedure with PBS/0.1% Tween 20 (Qbiogene Inc, Carlsbad, CA, USA) for 10 minutes. This step was

omitted for all extracellular stainings. Unspecific binding sites were blocked by incubation with 5% (v/v) FCS in PBS. Staining was achieved by overnight incubation with anti-AMPD2 antibody diluted in PBS at 4°C in the dark followed by a goat anti-rabbit secondary antibody diluted in PBS for two hours at RT. Actin was visualized using TRITC-conjugated phalloidin (1:50, Sigma-Aldrich, Cat# P1951, RRID:AB\_2315148) diluted in PBS/5% FCS for 40 minutes, whereas DAPI (1 µg/mL in PBS/5% FCS, 10-minute incubation) was applied to detect the nuclei. After three 3-minute washing steps with PBS images were acquired with an LSM 880 confocal laser scanning microscope (ZEISS, Germany, RRID:SCR\_020925) and a Bioevo BZ-9000 microscope (Keyence, RRID:SCR\_015486) and analyzed with ZEN (ZEISS) and ImageJ.

### 2.14 | Purine nucleoside measurements

CD14+ monocytes purified by MACS technology were incubated in RPMI without phenol red supplemented with 10% (v/v) human AB serum and 1 µg/mL LPS ±1 µg/mL BFA as indicated for 24 hours. Supernatants were collected and immediately stored at -80°C. Extracellular adenosine levels were determined enzymatically with the help of a fluorometric adenosine assay (abcam, Cat# ab211094) performed according to the manufacturer's instructions.

### 2.15 | Cytokine measurements

PBMCs were cultured in a 24-well plate in RPMI supplemented with 10% (v/v) heat-inactivated human AB serum at 10<sup>6</sup> cells per well. Incubation with either 100 µM / 1 mM ATP, 1 µM / 50 µM ADO, 100 µM / 1 mM IMP, or 100 µM / 1 mM inosine for 30 minutes was followed by immunostimulation with 1 µg/mL LPS for another two hours. Subsequently, supernatants were collected and TNF-alpha release was measured by ELISA (R&D Systems, Minneapolis, Minnesota, Cat# DY210, RRID:AB\_2848160).

### 2.16 | Statistical analysis

Statistical data analysis of mass spectrometric measurements was performed using Perseus software (v1.6.2.1). Technical and biological replicates for each condition were defined as groups and intensity values were filtered for "minimum value of 3" per group. After log<sub>2</sub> transformation missing values were imputed with random noise simulating the detection limit of the mass spectrometer. Imputed values are taken from a log normal distribution with 0.25× the standard deviation of the measured, logarithmized values, down-shifted by

1.8 standard deviations. Differential protein abundance was calculated using two-sample Student's *t* test, applying a permutation based FDR (false discovery rate) cut-off of 5%.

Statistical analyses of all other samples were performed using GraphPad Prism. In order to assess differences between paired samples Wilcoxon matched-pairs signed rank test was applied. Mann Whitney test was used to compare different groups.

## 2.17 | Search for potential membrane domains

UniProt and TMHMM servers were consulted to screen AMPD2 for potential transmembrane domains.<sup>80,81</sup> Subsequently, we followed the decision tree suggested by HeliQuest: The secondary protein structure was determined using the PSIPRED server.<sup>82,83</sup> The identified helical regions were then submitted to the HeliQuest webserver to calculate the hydrophobicity  $\langle H \rangle$ , the hydrophobic moment  $\langle \mu H \rangle$  and the net charge  $z$ . Based on these data, the discriminant factor  $D$  was then determined as follows:  $D = 0.944(\langle \mu H \rangle) + 0.33(z)$ .  $D > 1.34$  defined a lipid-binding helix, while helices with  $0.68 < D < 1.34$  were classified as possible lipid-binding helices.<sup>83,84</sup>

## 3 | RESULTS

### 3.1 | AMPD2 is differentially expressed in primary immune cells and various cell lines and is selectively detected on the cell surface

As AMPDs are encoded by three different genes, AMPD1, AMPD2, and AMPD3,<sup>85</sup> we initially aimed to determine the most abundant isoform in human immune cells. Data from the Human Protein Atlas reveals that AMPD2 represents the most common variant of AMPDs in human leukocytes (Figure 2A).<sup>86</sup> Consequently, we focused on this isoform in the following experiments. In order to identify a suitable model system to examine AMPD2 surface expression, we first analyzed cytoplasmic AMPD2 expression in different cell lines. Flow cytometric analysis following intracellular staining showed similar expression levels of AMPD2 in all examined cell lines, namely HEK293, HMEC-1, Jurkat, THP-1, and U-937 cells (Figure S2A, upper row). Cell lines generally displayed low eAMPD2 expression (Figure S2A, lower row). However, HEK293 cells and U-937 presented appreciable surface expression ( $r$  gMFI = 2.03 and 2.19) and a successful blocking of surface staining by an excess of unconjugated antibody and were thus chosen to further verify the presence of AMPD2 on the cell surface. Western blot analysis of AMPD2 immunoprecipitated from HEK293 and

U-937 membrane fractions additionally demonstrated the localization of AMPD2 in the cell membrane (Figure 2B). In order to confirm the identity of the immunoprecipitated target protein, mass spectrometric analyses of immunoprecipitated samples from HEK293 membrane fractions using a mouse monoclonal anti-AMPD2 antibody (QQ13) were performed. AMPD2 was found to be the top abundant protein (TopX) and was significantly enriched compared with isotype control ( $\log_2(\text{enrichment factor}) = 5.82$ ;  $-\log_{10}(P\text{-value}) = 3.85$  (LFQ)) (Figure S2C, Table S1). IP from HEK293 whole cell lysates using the staining antibody anti-AMPD2 (PA5) was performed in addition in order to validate antibody specificity by IP-MS (Table S1).<sup>87</sup> By concentrating the cytosolic and membrane lysates subsequently analyzed by SDS-PAGE, we were able to increase the amount of AMPD2 detected on western blot (Figure S2B). As our membrane protein purification procedure does not explicitly differentiate between plasma membrane and subcellular membranes, we conducted further experiments to characterize the membrane fraction: we detected both lamin B1 and calreticulin—markers of the nuclear membrane and the endoplasmic reticulum, respectively—in the purified membrane lysates (Figure S2D). Contamination by cytosolic protein indicated by GAPDH was, however, minimal (Figure S2D). As the presence of AMPD2 in the membrane fraction is, therefore, not clearly attributable to its presence in the plasma membrane, we performed surface biotinylation to verify the localization of AMPD2 at the cell surface. AMPD2 was detected in biotin-enriched samples isolated from HMEC-1 and U-937 cells as well as CD14+ monocytes by a surface biotinylation assay (Figure 2C). For HMEC-1 cells this result was verified with the help of mass spectrometry showing significant enrichment compared with non-biotinylated streptavidin-based pull-down controls ( $\log_2(\text{enrichment factor}) = 3.70$ ;  $-\log_{10}(P\text{-value}) = 2.00$  (LFQ)) (Figure 2D, Table S2). The top abundant proteins enriched by streptavidin-based pull-down following surface biotinylation are listed in Table S2 as proof of efficient surface protein enrichment. Figure S2E additionally shows flow-through samples to display surface abundance compared with the overall protein content. Surface biotinylation was also verified by flow cytometry demonstrating eAMPD2 expression on surface-biotinylated cells (Figure S2F). As Eltzhig et al previously demonstrated increased surface expression of adenosine deaminase in HMEC-1 cells exposed to hypoxia,<sup>88</sup> we additionally evaluated this scenario with respect to AMPD2. Interestingly, surface biotinylation of HMEC-1 cells cultured under hypoxic conditions revealed a slight decrease in AMPD2 surface expression (Figure S2G). Mass spectrometric analysis confirmed these results ( $\log_2(\text{enrichment factor}) = -0.44$  (LFQ);  $-\log_{10}(P\text{-value}) = 3.38$  (LFQ)). These data corresponded to flow cytometric analyses of the AMPD2 surface staining performed



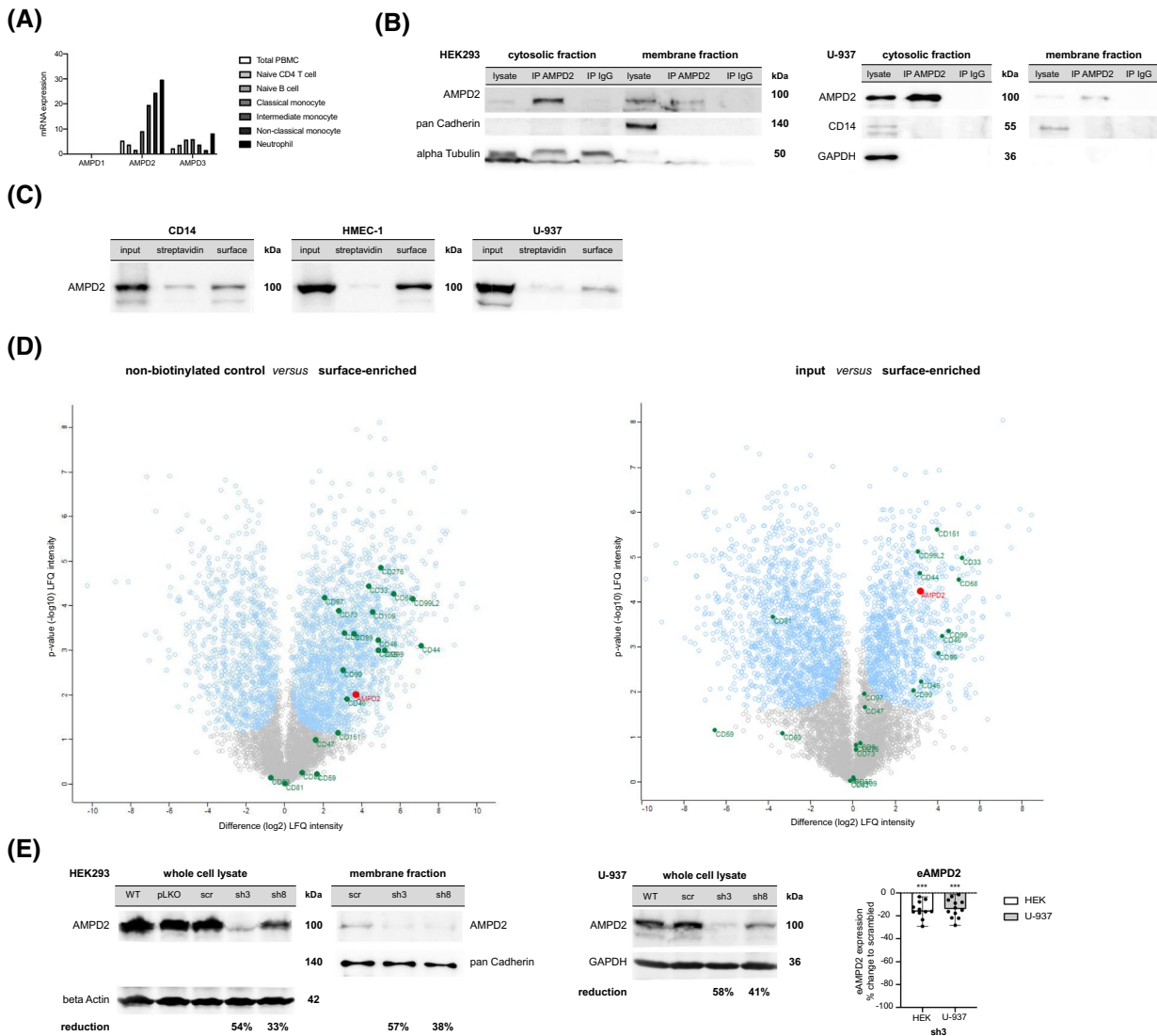


**FIGURE 2** Differential AMPD expression in primary human immune cells and cell lines and detection of AMPD2 in the cell membrane. A, mRNA expression of AMPD isoforms in human leukocyte populations according to the Human Protein Atlas.<sup>86</sup> The values represent normalized expression and were extracted from the Consensus dataset. B, Western blot analysis of AMPD2 pulled down from HEK293 and U-937 cytosolic and membrane fractions by IP using a mouse monoclonal antibody against human AMPD2 (IP AMPD2) compared to isotype control (IP IgG). Purity of cytosolic and membrane fractions was verified by analyzing pan Cadherin as well as alpha Tubulin and GAPDH, respectively. Uncropped images are provided in Figure S7. C, Western blot analysis of CD14+ monocytes, HMEC-1 and U-937 cells after surface protein enrichment. Surface biotinylation was performed followed by streptavidin-based pull-down (surface). A non-biotinylated control sample was run in parallel (streptavidin). Input samples represent cell lysates after surface biotinylation prior to streptavidin-based enrichment. D, Mass spectrometric analysis of surface-enriched protein obtained from HMEC-1 cells by streptavidin-based pull-down following surface biotinylation. Presence of AMPD2 in the surface-enriched fraction is displayed compared to streptavidin-based pull-down of non-biotinylated samples (non-biotinylated control) and biotinylated whole cell lysate without streptavidin-based pull-down (input), respectively. Differential protein abundance was determined using two-sample Student's *t* test and blue circles represent significance with an FDR cut-off of 5%. E, AMPD2 protein expression was quantified by western blot and flow cytometry. Western blot analysis of AMPD2 protein expression in HEK293 and U-937 whole cell lysates and HEK293 membrane fractions after AMPD2 knockdown by lentiviral transduction of shRNA particles and 10-day selection with 1  $\mu$ g/mL puromycin is shown on the left. AMPD2 protein expression was semiquantified relative to beta Actin, pan Cadherin and GAPDH, respectively, by image analysis and reduction by shRNA transduction is depicted in relation to a lentiviral negative control vector containing scrambled shRNA. BCA assay was utilized for protein quantification of membrane fractions. Uncropped images are provided in Figure S7. Reduced eAMPD2 surface expression in HEK293 and U-937 cells after lentiviral knockdown by shRNA sh3 was reproducible by surface staining and flow cytometric analysis ( $n = 11-12$ ). Doublets and dead cells were excluded for analysis as shown in Figure S1F. The data are depicted as change in *r* gMFI (geometric mean fluorescence intensity of staining to secondary antibody control) in relation to a lentiviral negative control vector containing scrambled shRNA. Bar graphs depict median and range. \*\*\* $P < .001$ , compared to scrambled shRNA; Wilcoxon matched-pairs signed rank test. WT, wild type; pLKO, pLKO.1 puro; scr, scrambled

in parallel (Figure S2G). Similarly, changes in CD73 expression observed under normoxic and hypoxic conditions measured by flow cytometry (Figure S2G) were consistent with the mass spectrometric analyses ( $\log_2(\text{enrichment factor}) = 0.566$  (LFQ);  $-\log_{10}(P\text{-value}) = 3.96$  (LFQ)). In summary, AMPD2 surface expression was confirmed by three independent methods in various cell lines.

### 3.2 | AMPD2 surface expression is reduced after AMPD2 knockdown in HEK293 and U-937 cells

In order to further substantiate surface staining specificity and verify eAMPD2 expression, we performed AMPD2 knockdown in HEK293 and U-937 cells. Knockdown efficiency was examined by transiently transfecting HEK293 cells with plasmids containing shRNA sequences targeting AMPD2. The corresponding sequences are listed in Table 1. Western blot analysis of whole cell lysates demonstrated that shRNA constructs 3 and 8 efficiently reduced AMPD2 protein expression. Thus, these shRNA sequences were used to produce viral particles and subsequently obtain stable gene silencing of AMPD2 by infecting HEK293 and U-937 cells. Successfully transduced cells were selected by puromycin and protein expression was analyzed by western blotting of whole cell lysates. Image analysis demonstrated that lentiviral knockdown with shRNA constructs 3 and 8 reduced AMPD2 protein expression by 54% and 33% in HEK293, and by 58% and 41% in U-937 cells (Figure 2E). In the following, AMPD2 protein levels were examined in membrane fractions from HEK293 cells stably expressing the viral constructs. Western blot analysis revealed that the reduction of AMPD2 in the membrane after stable gene silencing was similar to the changes observed with respect to the overall expression (Figure 2E). This reduction in membrane expression was reproduced by flow cytometric analysis following surface staining of successfully transduced HEK293 and U-937 cells (Figure 2E).

Sequence	H	$\mu\text{H}$	z	D
<sup>368</sup> NGPIKSFYRRLQYLSSK <sub>385</sub>	0.346	0.232	4	1.539008
<sup>369</sup> GPIKSFYRRLQYLSSKF <sub>386</sub>	0.479	0.338	4	1.639072
<sup>370</sup> PIKSFYRRLQYLSSKFQ <sub>387</sub>	0.467	0.346	4	1.646624
<sup>371</sup> IKSFYRRLQYLSSKFQM <sub>388</sub>	0.495	0.329	4	1.630576
<sup>372</sup> KSFYRRLQYLSSKFQMH <sub>389</sub>	0.402	0.248	4	1.554112

Note: Amino acids 368–389 of the AMPD2 protein sequence: H,  $\mu\text{H}$  and z were provided by the HeliQuest webserver.<sup>83</sup> D was calculated as follows:  $D = 0.944((\mu\text{H})) + 0.33(z)$ . A lipid-binding helix was defined by  $D > 1.34$ .

Abbreviations: D, discrimination factor; H, hydrophobicity; z, net charge;  $\mu\text{H}$ , hydrophobic moment.

### 3.3 | AMPD2 contains lipid-binding regions and AMPD2 surface expression is reduced by inhibitors of the secretory pathway

After verifying AMPD2 surface expression in different cell lines, we screened the proteins for potential membrane domains. UniProt and TMHMM servers did not identify any transmembrane domains in the protein sequence.<sup>80,81</sup> In order to search for lipid-binding regions that are characteristic of amphitropic proteins—proteins that localize both to the cytosol and to the plasma membrane—we identified helical regions with the help of the PSIPRED server.<sup>82</sup> The results of this search are displayed in Figure S2H. A total of 143 helical sequences were subsequently submitted to the HeliQuest webserver analyzing sequences containing 18 amino acids at a time in accordance with the server's requirements.<sup>83</sup> We identified five lipid-binding helices and 35 possible lipid-binding helices, although the identified sequences were overlapping due to the character of the search. Therefore, the five lipid-binding helices likely form part of one single lipid-binding region. The results are shown in Table 2 and Table S3. Additionally, we aimed to evaluate possible mechanisms of membrane trafficking experimentally: we verified whether changes in eAMPD2 expression could be provoked by disrupting protein transport via the Golgi apparatus. eAMPD2 expression was indeed reduced after treating HEK293 and U-937 cells with either 1  $\mu\text{g}/\text{mL}$  BFA or 0.5  $\mu\text{g}/\text{mL}$  MN for 24 hours (Figure S2I). Thus, we provide evidence that AMPD2 contains lipid-binding regions and that the secretory pathway is directly or indirectly involved in membrane trafficking of eAMPD2.

### 3.4 | AMPD2 is expressed on the cell surface of peripheral immune cells

Having successfully established a surface staining procedure in HEK293 and U-937 cells as model systems, we were particularly interested in examining its role in primary

**TABLE 2** Predicted lipid-binding region within the AMPD2 protein sequence

human immune cells. As expression of ectonucleotidases CD39 and CD73 has been described in a variety of immune cell populations,<sup>4</sup> our first endeavor was to screen different leukocyte subsets for eAMPD2 expression. Flow

cytometric analysis revealed that eAMPD2 was predominantly expressed on the cell surface of B cells, monocytes and granulocytes (Figure 3A). With respect to monocyte subpopulations, AMPD2 staining intensity did not differ

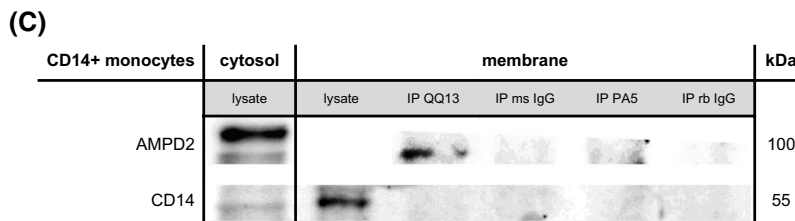
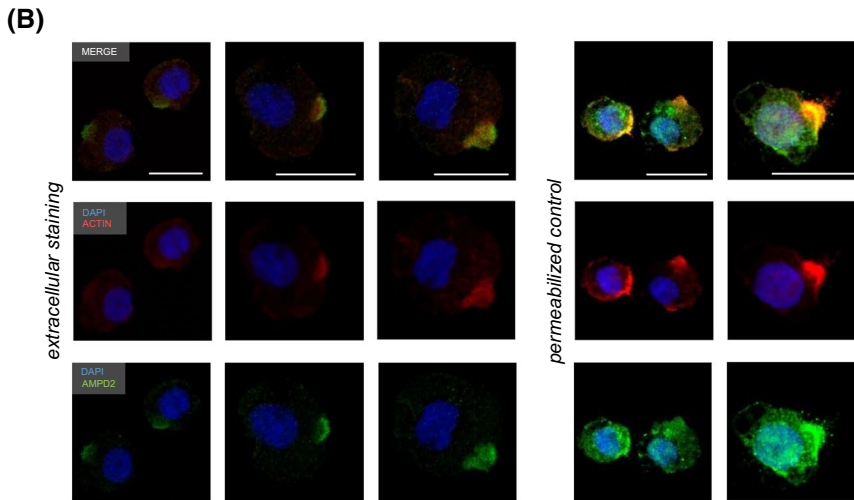
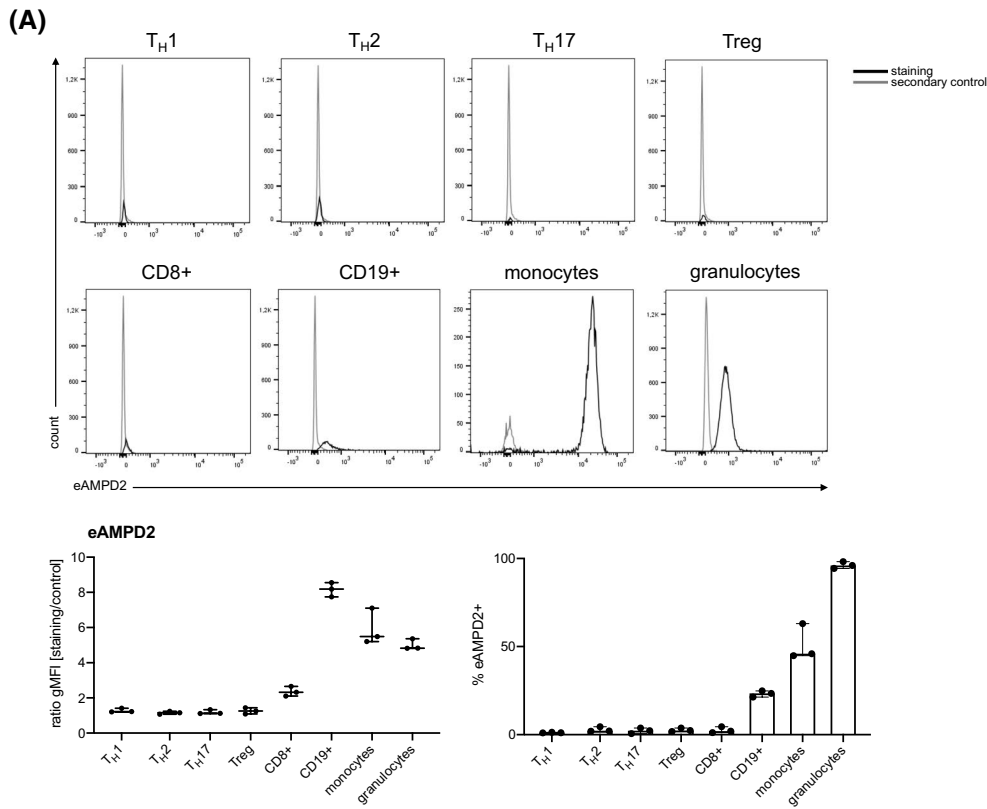


**FIGURE 3** AMPD2 surface expression on primary human immune cells. A, Human leukocytes were isolated by red blood cell lysis and analyzed for AMPD2 surface expression on different leukocyte subsets by flow cytometry ( $n = 3$ ). The gating strategy is displayed in Figure S1A. ratio gMFI represents the ratio of geometric mean fluorescence intensity of staining to secondary antibody control. B, Localization of AMPD2 on the cell surface of U-937 cells identified by immunofluorescence microscopy. Cells were stained for AMPD2 (green), actin (red) and DAPI (blue). The scale bar represents 20  $\mu\text{m}$ . The images show two independent experiments. Extracellular staining for eAMPD2 was performed on intact cells, while the cells were permeabilized to achieve intracellular staining. C, Western blot analysis of AMPD2 pulled down from membrane fractions of sorted CD14+ monocytes by IP using a mouse monoclonal antibody (QQ13) and a rabbit polyclonal antibody (PA5) against human AMPD2 compared to isotype control. CD14 was detected as a membrane marker. Uncropped images are provided in Figure S7. Boxplots show median and minimum or maximum values, respectively, while bar graphs depict median and range

between classical, intermediate and non-classical monocytes (Figure S1E). On the other hand, we did not observe significant expression of eAMPD2 in the different T cell populations examined, namely  $T_{H1}$ ,  $T_{H2}$ ,  $T_{H17}$  cells, Tregs and CD8+ T cells. Incubation with 25-fold excess unconjugated anti-AMPD2 antibody for 10 minutes completely prevented staining of the target protein, thus rebutting the possibility of the staining antibody inaccurately adhering to the cell surface (Figure S1E). Additionally, eAMPD2 expression on U-937 cells and PBMCs was confirmed by immunofluorescence microscopy as depicted in Figure 3B and Figure S3A. Actin as part of the cytoskeleton was visualized with the help of TRITC-conjugated phalloidin, while DAPI was applied to detect the cell nuclei. Incubation with rabbit IgG isotype control did not result in a signal (Figure S3A), whereas a distinct surface staining was achieved by adding anti-AMPD2 antibody. Furthermore, membrane fractions were prepared from isolated CD14+ monocytes. AMPD2 was successfully pulled down from the lysates by IP and detected by western blotting (Figure 3C). In comparison with equivalent samples incubated with corresponding isotype controls, AMPD2 was strongly enriched by IP performed with anti-AMPD2 antibodies (Figure 3C). The comparatively weak signal produced after pull-down with the polyclonal antibody “PA5” can be explained by the fact that this product is designed for flow cytometry. Significant enrichment of AMPD2 by IP from monocytic membrane fractions with mouse monoclonal anti-AMPD2 (QQ13) compared with isotype control was additionally confirmed by mass spectrometry ( $\log_2(\text{enrichment factor}) = 4.2$ ;  $-\log_{10}(P\text{-value}) = 2.87$  (LFQ)) (Table S4).

After verifying AMPD2 surface expression in primary immune cells and establishing a reliable surface staining, we proceeded to examine whether surface expression was modifiable by immunostimulation. As we could not refer to any previous data regarding eAMPD2 expression, we initially incubated PBMCs with 5  $\mu\text{g}/\text{mL}$  PHA-L and 1  $\mu\text{g}/\text{mL}$  LPS activating T lymphocytes and monocytes, respectively, and examined the kinetics of eAMPD2 expression for 30 hours. While eAMPD2 expression on lymphocytes tended to be reduced after incubation with PHA-L, we observed an increase in eAMPD2 on the cell surface of monocytes stimulated with LPS that reached a maximum after

20-24 hours (Figure S3E). In contrast, eAMPD2 expression was not enhanced in neutrophils activated by LPS stimulation (Figure S3B). Similarly, activating lymphocytes with a combination of PMA and ionomycin did not alter eAMPD2 expression (Figure S3C). Successful T cell stimulation was demonstrated by flow cytometric analysis of CD25 and CD69 (Figure S3D). Since we were specifically seeking conditions that augmented eAMPD2 expression to understand the role of this enzyme on the cell surface, we focused on monocytes in PBMC co-culture after 21-24 hours incubation in the following experiments. To guarantee that the enhanced surface staining after LPS stimulation was not caused by unspecific attachment of staining antibodies to dying monocytes upon activation, apoptotic and dead cells were excluded by dead cell removal as well as co-staining with annexin V. Both procedures did not affect the intensity of eAMPD2 expression measured by flow cytometry (Figure S3F). Therefore, we concluded that surface expression was in fact enhanced distinctively in stimulated monocytes, suggesting a possible role of eAMPD2 as a novel pro- or anti-inflammatory switch actively regulated by immune cells in states of inflammation.

### 3.5 | eAMPD2 and CD39 display a similar surface expression pattern

Following this first indication of its relevance, we aimed to further understand AMPD2 surface expression in the context of other ectoenzymes. Since we hypothesized a role in the ectonucleotidase-driven metabolism of extracellular purine nucleotides, we initially examined surface expression of eAMPD2, CD39 and CD73 by flow cytometry on human PBMCs at baseline (Figure S4A+B). Interestingly, CD73 was scarcely detectable on monocytes directly after isolation. Instead, we observed that CD73 expression was restricted to distinct lymphocyte subsets. CD73+ lymphocytes were predominantly identified as CD8+ T cells and CD19+ B cells (Figure S4D). Similar to eAMPD2, CD39 was predominantly expressed on monocytes, while only a small fraction of lymphocytes was CD39+. Indeed, eAMPD2 expression on monocytes tended to correlate with CD39 expression at baseline ( $r_{\text{Sp}} = 0.6788$ ,  $P = .0255$ ) (Figure S4B).

### 3.6 | TLR stimulation enhances AMPD2 surface expression on monocytes

In order to identify stimuli that enhance eAMPD2 expression, we next performed toll-like receptor (TLR) stimulation at TLRs 1-9 in PBMC co-culture. Except for Poly (I:C) and ODN 2006 that are agonists at TLR3 and TLR9, respectively, all reagents significantly enhanced eAMPD2 expression on human monocytes. The greatest increase in eAMPD2 expression compared with the untreated control was observed after stimulation of TLR4 and TLR7/8 (Figure 4B). A similar pattern was found regarding CD39 expression on monocytes, although agonists of TLR3 and TLR9 effectively enhanced CD39 surface expression as well (Figure 4B). Besides a slight reduction in CD73 surface expression on monocytes after incubation with the TLR9 agonist ODN 2006, CD73 expression was not significantly affected by TLR activation (Figure 4B). Lymphocytes were analyzed simultaneously and were largely unaffected by TLR stimulation. Although a significant reduction in CD73 expression was observed for each TLR agonist, these changes were minute (Figure 4A). Having confirmed LPS as the strongest trigger of eAMPD2 expression in monocytes, we proceeded to examine whether this increase could be prevented by Golgi transport inhibition; in order to confirm our prior hypothesis that the secretory pathway mediated AMPD2 surface expression. We observed that concomitant incubation with BFA significantly reduced eAMPD2 expression after 24 hours compared to LPS alone. This was true for both lymphocytes and monocytes in PBMC co-culture (Figure 4C+D). CD73 showed similar changes in monocytes, whereas surface expression proved to be more stable in lymphocytes (Figure 4C+D). Strikingly, disruption of the Golgi apparatus significantly increased monocytic CD39 surface expression (Figure 4D). Importantly, these effects were also observed for Golgi transport inhibition in the absence of concomitant immunostimulation (Figure 4C+D). Incubation with MN yielded similar results as BFA (Figure 4E+F). The effects observed in PBMC co-culture were successfully reproduced in a monoculture of isolated CD14+ monocytes (Figure 4E). Simultaneously, membrane fractions were generated from CD14+ monocytes and analyzed for AMPD2 protein expression by western blotting (Figure 4F). In accordance with the data acquired by flow cytometry, western blot analysis revealed an increase of approximately 35% in AMPD2 expression in membrane fractions of CD14+ monocytes stimulated with LPS. Of note, analysis of whole cell protein simultaneously demonstrated a decrease of total AMPD2 after LPS stimulation. Overall, we observed a significant increase in eAMPD2 expression on monocytes by TLR activation. This effect might either indicate a pro-inflammatory function of AMPD2 on the cell surface, maintaining a pro-inflammatory

environment by impeding adenosine production through CD73 in the extracellular space. On the other hand, similar to CD39, the upregulation by immunostimulation might equally represent a counter-regulatory mechanism to contain the state of inflammation.

### 3.7 | Dexamethasone inversely affects AMPD2 surface expression in lymphocytes and monocytes

Assuming that the enhancement of eAMPD2 expression by TLR agonism in monocytes constitutes a distinct immune cell response to immunoactivation, we hypothesized that these effects might be attenuated by the application of immunomodulatory drugs. First, we examined the impact of glucocorticoids (GC) as versatile anti-inflammatory agents broadly affecting various immune cell functions.<sup>89,90</sup> PBMCs were incubated with LPS as before and concomitantly treated with either  $10^{-8}$  M or  $10^{-5}$  M Dex. Contrary to our expectation, Dex treatment did not significantly prevent the increase in monocytic eAMPD2 expression by LPS stimulation (Figure 5A+B). The same was true with respect to CD39. However,  $10^{-5}$  M Dex tended to attenuate the enhancement of eAMPD2 ( $P = .05$ ). In order to adequately interpret these results, we also studied the effects of GC treatment in isolation. Flow cytometric analysis revealed that eAMPD2 expression was not affected by treatment with  $10^{-8}$  M Dex, a concentration that is equivalent to physiological glucocorticoid doses.<sup>91,92</sup> Notably, incubation with  $10^{-5}$  M Dex (corresponding to high-dose GC therapy)<sup>93,94</sup> resulted in a significant increase in eAMPD2 expression on monocytes while causing the opposite effect in lymphocytes in co-culture (Figure S5). A similar pattern was observed analyzing CD39 surface expression although the lower Dex concentration interestingly caused a decrease in CD39 in both populations. In contrast, CD73 surface expression was uniformly reduced by Dex. This effect was stronger in the presence of the lower concentration of Dex. Instead of reversing the effects of immunostimulation on monocytes, incubation with high doses of Dex consequently promoted a similar increase in the surface expression of both AMPD2 and CD39. We thus concluded that this upregulation might indeed represent an anti-inflammatory mechanism supported by GC treatment. As the immunomodulatory effects of MTX have been described to be partly modulated by changes in ectonucleotidase function,<sup>95-97</sup> we exploratorily examined PBMCs after incubation with  $0.8 \mu\text{M}$  MTX (corresponding to plasma levels achieved by weekly application of 15 mg MTX)<sup>98</sup> for 24 hours in comparison with untreated control samples or in the presence of LPS. We found that ectoenzyme expression remained unaffected by MTX treatment (Figure 5C+D).

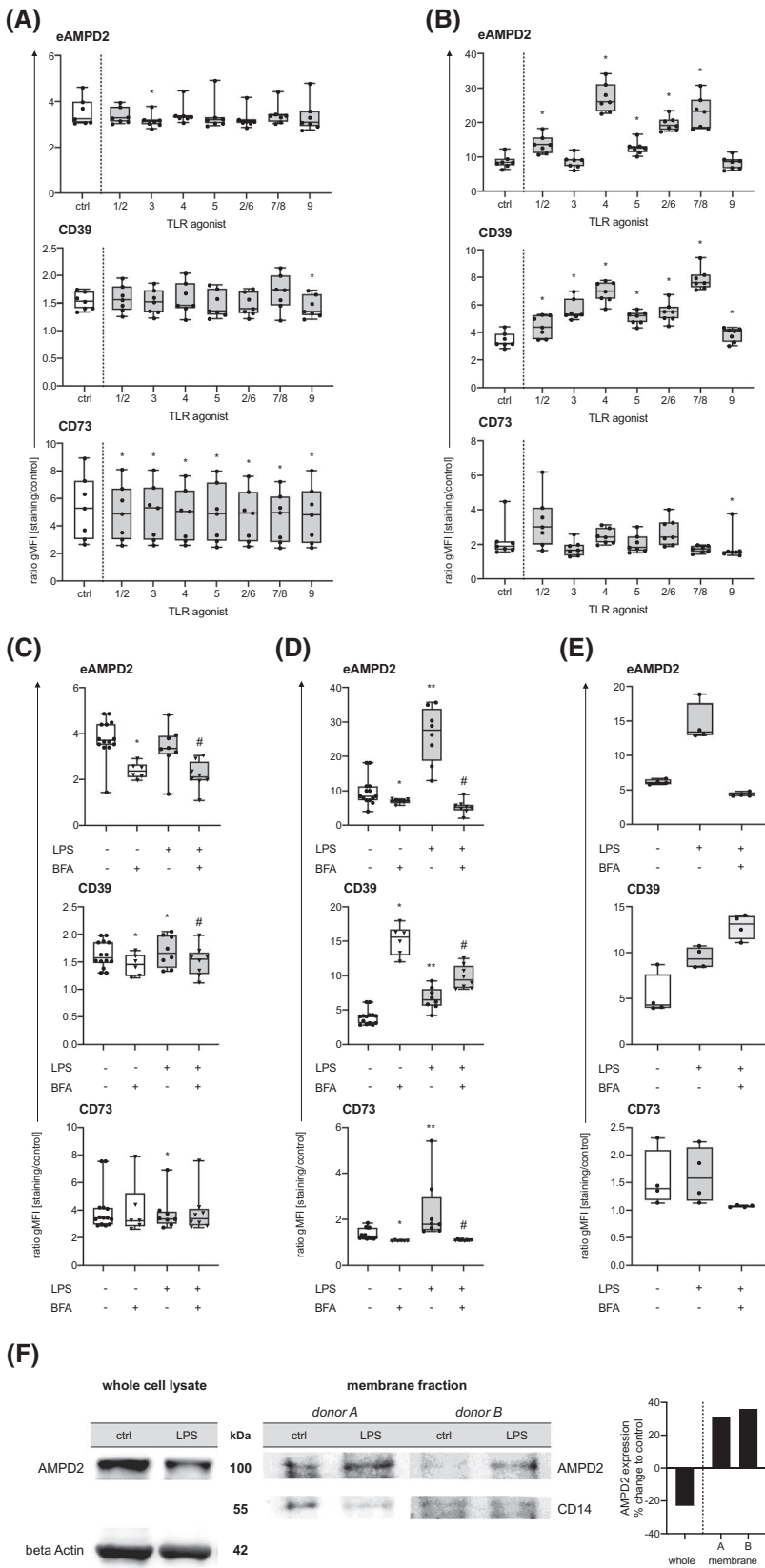


**FIGURE 4** AMPD2 surface expression on human PBMCs is altered by TLR stimulation and Golgi transport inhibition. Cells were incubated for 21-24 hours and surface expression of eAMPD2, CD39 and CD73 was measured by flow cytometry. TLR agonism was achieved using 1  $\mu$ g/mL Pam3SCK4 at TLR1/2, 10  $\mu$ g/mL Poly (I:C) at TLR3, 1  $\mu$ g/mL LPS at TLR4, 100 ng/mL Flagellin at TLR5, 1  $\mu$ g/mL FSL-1 at TLR2/6, 1  $\mu$ g/mL at TLR7/8, and 0.5  $\mu$ M ODN 2006 at TLR9. 1  $\mu$ g/mL BFA was added simultaneously as indicated to inhibit Golgi transport. Lymphocytes (A,C) and monocytes (B,D) were incubated in co-culture and gated according to Figure S1E for analysis (n = 7-8). E, CD14+ monocytes were sorted by magnetic cell separation and incubated in monoculture (n = 4). The applied gating strategy is depicted in Figure S1B. ratio gMFI represents the ratio of geometric mean fluorescence intensity of staining to secondary antibody control. F, AMPD2 protein expression in sorted CD14+ monocytes was detected by western blotting of whole cell lysates and membrane fractions after 24-hour incubation with 1  $\mu$ g/mL LPS. AMPD2 protein expression was semiquantified relative to beta Actin and CD14 respectively by image analysis and modification by LPS stimulation is depicted in relation to a untreated control samples. All boxplots show median, interquartile range, and minimum or maximum values, respectively. \* $P$  < .05, \*\* $P$  < .01, compared to untreated control; # $P$  < .01, compared to LPS; Wilcoxon matched-pairs signed rank test

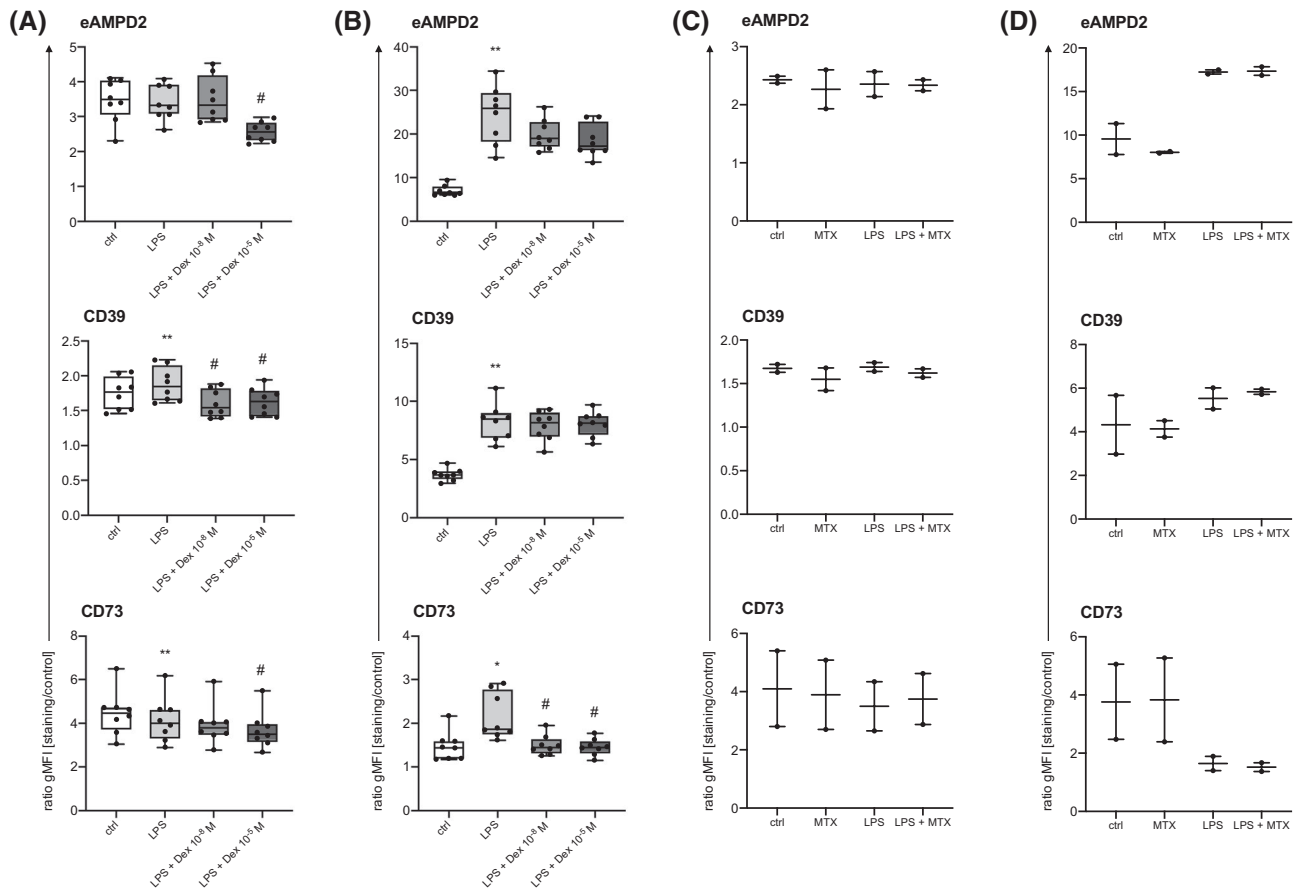


**FIGURE 5** AMPD2 surface expression on human PBMCs following immunomodulation. Cells were incubated for 21–24 hours and surface expression of eAMPD2, CD39 and CD73 was measured by flow cytometry. Lymphocytes (A,C) and monocytes (B,D) were incubated in co-culture and gated according to Figure S1E for analysis. ratio gMFI represents the ratio of geometric mean fluorescence intensity of staining to secondary antibody control. A,B, PBMCs were treated with 1  $\mu\text{g}/\text{mL}$  LPS  $\pm 10^{-8}$  and  $10^{-5}$  M dexamethasone, respectively ( $n = 8$ ). C,D, PBMC co-cultures were incubated with 0.8  $\mu\text{M}$  methotrexate and 1  $\mu\text{g}/\text{mL}$  LPS, respectively, and a combination of both ( $n = 2$ ). All boxplots show median, interquartile range, and minimum or maximum values, respectively. \* $P < .05$ , \*\* $P < .01$ , compared to untreated control; # $P < .01$ , compared to LPS; Wilcoxon matched-pairs signed rank test

### 3.8 | Patients with rheumatoid arthritis show increased AMPD2 surface expression in peripheral blood lymphocytes and monocytes

Having confirmed that eAMPD2 expression was distinctively modified by immunoactivation *in vitro*, we investigated whether eAMPD2 was equally affected by inflammatory conditions *in vivo*. Therefore, we isolated PBMCs from peripheral blood samples from patients with RA and healthy controls. Patient characteristics are provided in Table 3. The majority of patients were under immunosuppressive therapy. Sex and age distribution in the healthy control group did not differ significantly from the patient group (Table 3). Surface expression of AMPD2, CD39 and CD73 was examined by flow cytometry. Comparing PBMCs at baseline, we observed that eAMPD2 expression in RA patients was significantly elevated compared with healthy controls (Figure 6A). Remarkably, this was true for both lymphocytes and monocytes. This enhancement did not correlate with CRP levels

indicating inflammatory activity nor with the current GC dose, although a reliable correlation analysis would require a greater sample size. Contrary to our previous results, CD39 expression in monocytes was not correspondent with eAMPD2 in this experiment where no differences between RA patients and healthy controls were apparent (Figure 6A). Lymphocytes, on the other hand, showed significantly lower levels of CD39 expression (Figure 6A) although the overall expression was low and lymphocyte subsets would have to be analyzed separately to properly evaluate the relevance of this finding. CD73 expression was not significantly different between the two groups (Figure 6A). Regarding CD73, we found that monocytic expression was generally very low at baseline immediately after isolation and increased in cell culture. These findings are discussed more thoroughly in the Appendix.

After confirming differences in baseline expression of eAMPD2, we were interested whether expression patterns in PBMCs from RA patients also differed from healthy controls

**TABLE 3** Patient characteristics

Patients, n	15
Healthy controls	13
Female, n (%)	11 (73)
Healthy controls	8 (62)
Age [years], median (IQR)	61 (54-73)
Healthy controls	56 (51-75)
Disease duration [years], median (IQR)	17 (8.5-32)
RF-positive, n (%)	10 (67)
Anti-CCP-positive, n (%)	10 (67)
CRP [mg/L], median (IQR)	5 (1.1-6.5) <sup>a</sup>
ESR 1st hour [mm/h], median (IQR)	18 (9.5-35) <sup>b</sup>
SJC [n/28], median (IQR)	2 (0.5-3.5) <sup>b</sup>
TJC [n/28], median (IQR)	1 (0-4.5) <sup>b</sup>
Receiving DMARDs, n (%)	12 (80)
Receiving GCs, n (%)	11 (73)
Current GC dose [mg/d PE], median (IQR)	5 (3-10) <sup>c</sup>

Abbreviations: CCP, cyclic citrullinated peptide; CRP, C-reactive protein; DMARDs, disease-modifying anti-rheumatic drugs; ESR, erythrocyte sedimentation rate; GC, glucocorticoids; IQR, interquartile range; PE, prednisone equivalent; RF, rheumatoid factor; SJC, swollen joint count; TJC, tender joint count.

<sup>a</sup>Information available for 12/15.

<sup>b</sup>Information available for 9/15.

<sup>c</sup>Calculated only for patients receiving glucocorticoids.

in response to in vitro stimulation. Cells were incubated with LPS as before and surface expression of AMPD2, CD39 and CD73 was assessed by flow cytometry after 24 hours. Overall, the response to LPS in PBMCs from RA patients resembled that of healthy controls (Figure 6B). However, contrary to corresponding samples from healthy controls, several patients did not exhibit an increase in monocytic surface expression of AMPD2 ( $P = .14$ ) and CD39 ( $P = .05$ ). With respect to eAMPD2, we concluded that elevated surface expression in monocytes at baseline represents a counter-regulatory mechanism in response to the inflammatory state prevalent in RA. We assumed that this permanent upregulation impedes any further increase in eAMPD2 expression upon in vitro stimulation. While changes in CD73 expression did not differ between stimulated monocytes from healthy controls and RA patients, we did nevertheless observe a striking difference compared with the expression pattern in our previous measurements where LPS stimulation generally increased monocytic CD73 expression (Figure 4D). Comparing the characteristics of healthy donors in these experiments, it became evident that the age distribution was significantly different between the two groups ( $P = .003$ ). For this reason, we reanalyzed our data by dividing the healthy donors into two groups ( $\leq 40$  years and  $\geq 50$  years) (Table S5). Interestingly, we found that ectoenzyme expression in monocytes stimulated with LPS was indeed regulated significantly differently

in young and old donors (Figure S6B). In comparison with the younger group, monocytes from older individuals showed a significantly weaker upregulation of AMPD2, CD39 and CD73 surface expression. Differences between the two groups were also apparent at baseline (Figure S6A).

In conclusion, our data showed that eAMPD2 was differentially regulated in both RA and aging—two states associated with distinct patterns of inflammation. We thus concluded that eAMPD2 might indeed exert an immunoregulatory function by modifying the extracellular balance of purine metabolites.

### 3.9 | Increased AMPD2 surface expression does not prevent extracellular adenosine production

According to our initial hypothesis, we assumed that eAMPD2 might in fact exhibit either a pro-inflammatory or an anti-inflammatory role in the extracellular space. By metabolizing AMP to IMP, the deaminase processes the product of CD39 action, thereby shifting the balance of this reaction and enabling further degradation of ATP by the ectonucleotidase. This reduction of pro-inflammatory ATP favors a predominantly anti-inflammatory role of surface AMPD2. On the other hand, AMP also represents the substrate of ADO generation by CD73. AMP depletion by AMPD2 might therefore equally cause a reduction in eADO—a very potent anti-inflammatory molecule.<sup>56</sup> In order to evaluate the likelihood of either scenario, we isolated CD14+ monocytes from PBMCs by magnetic cell separation and incubated the cells with 1  $\mu\text{g}/\text{mL}$  LPS  $\pm$  1  $\mu\text{g}/\text{mL}$  BFA for 24 hours. Supernatants were collected after 24 hours and surface expression of eAMPD2, CD39 and CD73 was determined by flow cytometry (Figure 4E). Fluorometric measurements of ADO in the supernatant revealed that an increase in eAMPD2 expression was not associated with a decrease in eADO (Figure 6C). In contrast, stimulation with LPS demonstrated maximal eAMPD2 expression (Figure 4E) and the highest levels of ADO in the supernatant (Figure 6C). CD73 expression was also at the maximum under these conditions and certainly contributed to the increase in eADO production. Similarly, a decrease in the ecto-5'-nucleotidase was presumably responsible for the reduction in eADO observed after Golgi transport inhibition. Moreover, immune cell activation and death considerably affect extracellular purine metabolite levels so that immunostimulation might cause changes in eADO levels independent of ectoenzyme expression.<sup>9,16,18,19,99</sup> However, the percentage of dead cells did not differ between cells stimulated with LPS only or a combination of LPS and BFA. While this assay is consequently not suitable to exclusively measure eAMPD2 action, the results nevertheless refute the hypothesis that enhanced expression of eAMPD2 on the cell



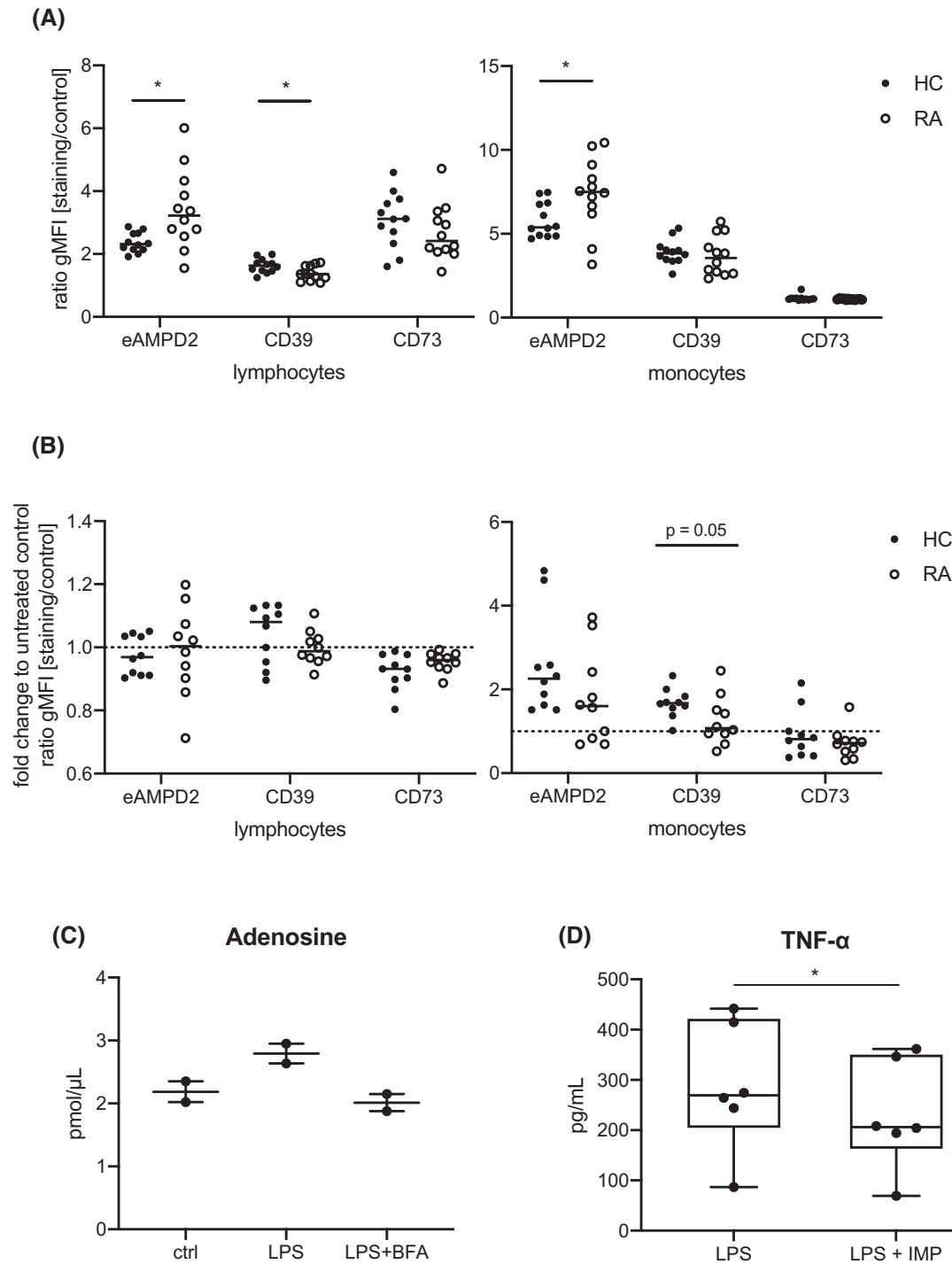


**FIGURE 6** eAMPD2 expression on PBMCs from RA patients and functional assays suggest an anti-inflammatory potential of AMPD2 surface expression. A, eAMPD2, CD39 and CD73 surface expression was analyzed by flow cytometry directly after isolation ( $n = 12$ ). PBMCs were gated according to Figure S1E for analysis. ratio gMFI represents the ratio of geometric mean fluorescence intensity of staining to secondary antibody control. B, Flow cytometric analysis of eAMPD2, CD39 and CD73 surface expression after incubation with 1  $\mu$ g/mL LPS for 21-24 hours in co-culture ( $n = 10$ ). PBMCs were gated according to Figure S1E for analysis. Modification by LPS stimulation is depicted in relation to untreated control samples. C, CD14 $^{+}$  monocytes were purified from human PBMCs by MACS technology and incubated with 1  $\mu$ g/mL LPS  $\pm$  1  $\mu$ g/mL BFA for 24 hours. The concentration of adenosine in the supernatant was determined using a fluorometric assay ( $n = 2$ ). D, TNF-alpha release determined by ELISA. PBMCs were preincubated with 100  $\mu$ M IMP for 30 minutes, 1  $\mu$ g/mL LPS was added for another 2 hours ( $n = 6$ ). Lines on scatter dot plot represent median. Boxplots show median, interquartile range, and minimum or maximum values, respectively. \* $P < .05$ , Mann Whitney test (A+B) and Wilcoxon matched-pairs signed rank test (C+D). IMP, inosine 5'-monophosphate

surface prevents production of anti-inflammatory ADO in the extracellular space.

### 3.10 | Inosine monophosphate—the product of AMPD2 action—exerts anti-inflammatory effects

In the system of extracellular purine metabolism regulated by the ectonucleotidases CD39 and CD73, the element that is newly introduced by the discovery of AMPD2 surface expression is the extracellular production of IMP. While the role of eATP and eADO has been studied in detail, the function of inosine derivatives in the interstitial space is less certain.<sup>6,13,56,100,101</sup> For this reason, we aimed to examine the potential of excess extracellular IMP in balancing inflammation. PBMCs were primed with low and high supraphysiological concentrations of different purine metabolites and subsequently stimulated with 1 µg/mL LPS for two hours. Purine metabolites were applied at concentrations detected in the extracellular space under inflammatory conditions as described previously.<sup>102-111</sup> The ADO concentrations applied also corresponded with the levels measured in our own experiments in the supernatant of cultured immune cells (Figure 6C). TNF-alpha was measured in the supernatants as an indicator of inflammatory activity. Prior incubation with 100 µM IMP significantly reduced TNF-alpha release from PBMCs after LPS stimulation (Figure 6D). We therefore concluded that eAMPD2 exerts anti-inflammatory effects by production of extracellular IMP and is upregulated upon immunoactivation to contain the inflammatory environment. As expected, ADO also exhibited highly efficient anti-inflammatory activity ( $P = .03$ ). In comparison, inosine was less potent in reducing TNF-alpha release ( $P = .22$ ). Surprisingly, ATP resulted in the strongest decrease in TNF-alpha release ( $P = .03$ ). This effect was contrary to the pro-inflammatory activity usually attributed to eATP.<sup>102</sup> Considering the ample expression of ectoenzymes in PBMCs, this finding can nevertheless be accounted for by an increase in ADO and IMP production by supplying ATP as a substrate.

## 4 | DISCUSSION

In this study, we verified AMPD2 surface expression in primary human immune cells and assessed differences in expression in patients with RA. Through a combination of mass spectrometry from membrane fractions and surface staining procedures, we identified eAMPD2 as a novel ectoenzyme involved in the extracellular purine metabolism. Immunostimulation increased monocytic eAMPD2 expression and RA patients exhibited higher surface expression

levels at baseline. This upregulation was not associated with a decrease in eADO levels in cell culture, while IMP exerted anti-inflammatory effects on immune cells.

By confirming AMPD2 surface expression in immune cells, we pursued a concept that was first discussed over 50 years ago in muscle tissue.<sup>63,64</sup> Contrary to Rao and Pipoly who described attachment of AMPD to the inner erythrocyte membrane,<sup>65,66</sup> we found that AMPD2 is indeed expressed on the outer surface and consequently potentially relevant to the extracellular milieu. While CD39 and CD73 are integrated into the plasma membrane by transmembrane domains and a GPI anchor, respectively,<sup>112,113</sup> UniProt and TMHMM queries revealed no corresponding motifs in the AMPD2 protein sequence.<sup>80,81</sup> In order to further elucidate membrane trafficking of eAMPD2, we analyzed surface expression after Golgi transport inhibition and observed a significant reduction suggesting involvement of the secretory pathway in the surface localization of eAMPD2. These results are in line with previous data locating AMPD in subcellular membrane fractions.<sup>114,115</sup> Sims et al identified pleckstrin homology domains that might mediate membrane-association via phosphoinositide binding in both AMPD2 and AMPD3.<sup>116</sup> Similarly, our search identified a lipid-binding region in the AMPD2 protein sequence. These helical domains are characteristic of amphitropic proteins—a class first described by Burn in 1988.<sup>84,117</sup> This group of cytosolic proteins displays structural features that enable a reversible interaction with the plasma membrane.<sup>118,119</sup> The presence of a lipid-binding helix therefore represents a potential mechanism permitting eAMPD2 to associate with the membrane. Further work will be needed to understand this process in detail.

Since the expression pattern of CD39 and CD73 differs between immune cell subsets, we determined eAMPD2 expression in various leukocyte populations.<sup>4</sup> We found that eAMPD2 expression intensities resembled the distribution of CD39 described previously. These findings suggest that eAMPD2 might assist CD39 activity by shifting the ATP:AMP ratio and hence promoting hydrolysis of pro-inflammatory ATP by CD39. This theory is further supported by the fact that monocytic eAMPD2 expression correlated with CD39. Similarly, we observed an upregulation in both eAMPD2 and CD39 in monocytes upon TLR stimulation. According to our hypothesis, this upregulation under inflammatory conditions might be beneficial by containing ATP signaling and thereby attenuating a potentially detrimental inflammatory response. In accordance with this concept, CD39 deficient mice exhibited increased levels of vascular inflammation.<sup>120</sup> Conversely, transducing fibroblast-like synoviocytes with CD39 and CD73 resulted in reduced secretion of pro-inflammatory cytokines.<sup>121</sup> Moreover, an induction of AMPD2 had been previously described in chondrocytes upon exposure to IL-1β.<sup>122</sup> Since these changes in overall AMPD2 protein expression were reversed by incubation with immunomodulatory

agents, we evaluated whether eAMPD2 upregulation was also mitigated by anti-inflammatory therapeutics. Although Dex slightly attenuated the increase in eAMPD2 expression in monocytes upon stimulation with LPS, these changes were however not significant. Interestingly, exposure to therapeutic concentrations of Dex alone significantly increased monocytic eAMPD2 expression. We concluded that eAMPD2 upregulation might thus mediate anti-inflammatory effects of Dex in the extracellular space. Indeed, AMPD2 and AMPD3 have previously been recognized as genes addressed by glucocorticoid receptor signaling.<sup>123,124</sup> The discrepant effects of Dex on monocytic eAMPD2 expression observed in the presence and absence of concomitant immunostimulation might reflect the attenuation of the inflammatory stimuli in the first scenario as opposed to the direct impact of Dex on AMPD2 surface expression in the latter. A reduction in eAMPD2, CD39 and CD73 expression was observed in the lymphocyte population. In contrast, previous studies of specific lymphocyte subsets demonstrated an increase in both CD39 and CD73 expression caused by Dex treatment.<sup>125-128</sup> Likewise, the mechanism of action of MTX has been attributed to changes in AMPD activity.<sup>129,130</sup> However, contrary to Dex, the anti-inflammatory effect in this context is not ascribed to a facilitation of ATP degradation, but rather to an inhibition of AMPD causing increased levels of eADO.<sup>95</sup> Correspondingly, polymorphisms causing reduced AMPD activity were associated with enhanced responsiveness to MTX, while low CD39 expression in Tregs caused the opposite.<sup>131,132</sup> Bossennec et al found that MTX treatment was indeed associated with increased ADO production by T<sub>H</sub> cells from RA patients.<sup>96</sup> Nevertheless, we did not observe changes in eAMPD2 expression after incubation with MTX. Importantly, it has to be considered that—in vivo—several immunomodulatory effects only manifest after up to three months of MTX therapy.<sup>133</sup> Also, the proposed mechanism of MTX action only refers to cytosolic AMPD activity. While we focused on eAMPD2 expression, it would be desirable to perform analyses of eAMPD2 function under MTX treatment in the future.

Differences in ectonucleotidase expression have been observed in various immune-mediated diseases. On the one hand, an elevated expression of CD39, CD73 and A2AR, respectively, has been described in neutrophils and monocytes from the synovial fluid of mice with collagen-induced arthritis and the peripheral blood of patients with uveitis.<sup>38,51</sup> Also, FOXP3+CD39+ Tregs were found to be enriched in the synovial tissue of RA patients.<sup>134</sup> On the other hand, decreased expression of CD39, A1R and A2BR was detected in patients with ankylosing spondylitis and CD73 was downregulated on Tregs from psoriasis patients.<sup>49,50</sup> Likewise, a reduction in ADO formation was observed in the synovial fluid of patients with juvenile idiopathic arthritis.<sup>48</sup> These diverging results indicate both a potential dysregulation of

ectonucleotidase expression enhancing inflammation by impaired eADO production and a counter-regulatory increase in CD39 and CD73 expression to attenuate the pro-inflammatory response in autoimmune diseases. Compared with sex- and age-matched healthy controls we observed higher levels of eAMPD2 expression in both lymphocytes and monocytes from RA patients. Interestingly, monocytic CD39 expression did not differ in our cohort. In response to TLR4 stimulation, upregulation of eAMPD2 in monocytes was not significantly different in the two groups, although it tended to be lower in RA patients. This is in line with the increased baseline levels, preventing further upregulation following a pro-inflammatory stimulus. As stated before, increased levels of eAMPD2 expression might constitute a counter-regulatory mechanism, promoting the removal of immunostimulatory ATP and providing anti-inflammatory IMP. AMPD activity has indeed been shown to correlate inversely with ATP levels.<sup>135-137</sup> Importantly, our RA cohort comprises a diverse population that does not allow for the differential assessment of the impact of disease activity and current immunosuppressive therapy. Similarly, further experiments will be necessary to determine the relevance of the age-related differences observed in our cohort and ensure that the results were not caused by confounding factors like comorbidities. On the other hand, eAMPD2 may equally represent an ambiguous mediator of the extracellular ATP-adenosine balance by simultaneously reducing AMP supply and thereby impairing eADO generation. In fact, contrary to our findings in RA patients, Guo et al detected decreased overall AMPD2 protein levels in SLE patients.<sup>138</sup>

Consequently, we aimed to evaluate whether modifying eAMPD2 expression was indeed associated with changes in extracellular eADO content. We did not observe a reduction in eADO concentrations under conditions of increased eAMPD2 expression. Thus, we concluded that impairing anti-inflammatory ectonucleotidase function does not seem to be the dominant role of eAMPD2. However, our approach only represents an approximation of eAMPD2 activity and does not exclude the action of other ectoenzymes present in the experimental setup. A more precise analysis of eAMPD2 function will be advantageous to define the exact role of eAMPD2 in the extracellular purine metabolism: direct measurements of extracellular AMP and IMP levels and the use of specific inhibitors will be necessary to characterize the enzymatic function on the cell surface. In order to provide an initial concept of the immunoregulatory capacity of extracellular AMP deamination, we exploratorily examined the anti-inflammatory effects of IMP and inosine in comparison to adenine nucleotides. IMP was indeed capable of reducing TNF- $\alpha$  secretion from PBMCs upon TLR4 stimulation, supporting the immunomodulatory potential of extracellular AMPD2 activity. Our results are in agreement with previous findings highlighting the anti-inflammatory

potency of inosine. Inosine has been shown to signal via ADO receptors.<sup>111,139-141</sup> Immunosuppressive effects of inosine have been observed in multiple leukocyte populations including T cells, monocytes, neutrophils and macrophages.<sup>109,142,143</sup> Moreover, Qiu et al demonstrated that IMP exhibited anti-inflammatory potential by inhibiting neutrophil accumulation.<sup>144</sup> The additional benefit of inosine derivatives in the extracellular space might consist in their longevity. Compared with the very short-lived ADO (half-life: 10 seconds), the half-life of inosine has been defined as 15 hours.<sup>145,146</sup> While ADO might serve as an immediate regulator with strong anti-inflammatory potential, inosine nucleotides might permit a more prolonged modulation of the inflammatory environment.

In conclusion, we provide evidence of AMPD2 surface expression in human primary immune cells for the first time and thereby introduce a novel regulator of the extracellular purine metabolism that is differentially regulated under inflammatory conditions. We propose that an upregulation of eAMPD2 might enhance the removal of pro-inflammatory ATP from the extracellular space, although further work will be required to elucidate the precise function of this novel ectoenzyme in the inflammatory microenvironment. Considering the promising role of therapeutic agents in advancing the treatment of both immune-mediated and oncological diseases, we regard our findings as an important advancement expanding the system of immunoregulatory ectonucleotidases.

## ACKNOWLEDGMENTS

We acknowledge funding provided by an unrestricted grant from Horizon Pharma plc. (112517). This work was supported by grants from Horizon Pharma plc. (112517) for LE, Studienstiftung des deutschen Volkes (Alexandra Damerau) for AD, and Deutsche Forschungsgemeinschaft (353142848) for TG.

## CONFLICT OF INTEREST

The authors have no financial conflicts of interest.

## AUTHOR CONTRIBUTIONS

We declare that all authors included on this paper fulfill the criteria of authorship. L. Ehlers, C. Strehl, F. Buttgerit and T. Gaber designed the research agenda; L. Ehlers, A. Kuppe, A. Damerau and S. Wilantri performed the experiments and analyzed the data; M. Kirchner and P. Mertins performed the mass spectrometric analyses; L. Ehlers wrote the paper. All authors have read and approved the final manuscript.

## ORCID

Lisa Ehlers  <https://orcid.org/0000-0001-8737-001X>

## REFERENCES

1. Antonioli L, Csóka B, Fornai M, et al. Adenosine and inflammation: what's new on the horizon? *Drug Discov Today*. 2014;19(8):1051-1068.
2. Antonioli L, Novitskiy SV, Sachsenmeier KF, Fornai M, Blandizzi C, Haskó G. Switching off CD73: a way to boost the activity of conventional and targeted antineoplastic therapies. *Drug Discov Today*. 2017;22(11):1686-1696.
3. Reutershan J, Vollmer I, Stark S, Wagner R, Ngamsri KC, Eltzschig HK. Adenosine and inflammation: CD39 and CD73 are critical mediators in LPS-induced PMN trafficking into the lungs. *FASEB J*. 2009;23(2):473-482.
4. Antonioli L, Pacher P, Vizi ES, Haskó G. CD39 and CD73 in immunity and inflammation. *Trends Mol Med*. 2013;19(6):355-367.
5. Horenstein AL, Chillemi A, Zaccarello G, et al. A CD38/CD203a/CD73 ectoenzymatic pathway independent of CD39 drives a novel adenosinergic loop in human T lymphocytes. *OncoImmunology*. 2013;2(9):e26246.
6. Ferretti E, Horenstein AL, Canzonetta C, Costa F, Morandi F. Canonical and non-canonical adenosinergic pathways. *Immunol Lett*. 2019;205:25-30.
7. Dong RP, Kameoka J, Hegen M, et al. Characterization of adenosine deaminase binding to human CD26 on T cells and its biologic role in immune response. *J Immunol*. 1996;156(4):1349-1355.
8. Eltzschig HK, Eckle T, Mager A, et al. ATP release from activated neutrophils occurs via connexin 43 and modulates adenosine-dependent endothelial cell function. *Circ Res*. 2006;99(10):1100-1108.
9. Qu Y, Misaghi S, Newton K, et al. Pannexin-1 is required for ATP release during apoptosis but not for inflammasome activation. *J Immunol*. 2011;186(11):6553-6561.
10. Baldwin SA, Beal PR, Yao SY, King AE, Cass CE, Young JD. The equilibrative nucleoside transporter family, SLC29. *Pflugers Arch*. 2004;447(5):735-743.
11. Gray JH, Owen RP, Giacomini KM. The concentrative nucleoside transporter family, SLC28. *Pflugers Arch*. 2004;447(5):728-734.
12. Antonioli L, Blandizzi C, Pacher P, Haskó G. Immunity, inflammation and cancer: a leading role for adenosine. *Nat Rev Cancer*. 2013;13(12):842-857.
13. Dou L, Chen YF, Cowan PJ, Chen XP. Extracellular ATP signaling and clinical relevance. *Clin Immunol*. 2018;188:67-73.
14. Cronstein BN, Sitkovsky M. Adenosine and adenosine receptors in the pathogenesis and treatment of rheumatic diseases. *Nat Rev Rheumatol*. 2017;13(1):41-51.
15. Antonioli L, Colucci R, La Motta C, et al. Adenosine deaminase in the modulation of immune system and its potential as a novel target for treatment of inflammatory disorders. *Curr Drug Targets*. 2012;13(6):842-862.
16. Elliott MR, Chekeni FB, Trampont PC, et al. Nucleotides released by apoptotic cells act as a find-me signal to promote phagocytic clearance. *Nature*. 2009;461(7261):282-286.
17. Trautmann A. Extracellular ATP in the immune system: more than just a "danger signal". *Sci Signal*. 2009;2(56):pe6.
18. Chen Y, Corriden R, Inoue Y, et al. ATP release guides neutrophil chemotaxis via P2Y2 and A3 receptors. *Science*. 2006;314(5806):1792-1795.
19. Schenk U, Westendorf AM, Radaelli E, et al. Purinergic control of T cell activation by ATP released through pannexin-1 hemichannels. *Sci Signal*. 2008;1(39):ra6.

20. Ferrari D, Chiozzi P, Falzoni S, et al. Extracellular ATP triggers IL-1 beta release by activating the purinergic P2Z receptor of human macrophages. *J Immunol.* 1997;159(3):1451-1458.
21. MacKenzie A, Wilson HL, Kiss-Toth E, Dower SK, North RA, Surprenant A. Rapid secretion of interleukin-1beta by microvesicle shedding. *Immunity.* 2001;15(5):825-835.
22. Pelegrin P, Barroso-Gutierrez C, Surprenant A. P2X7 receptor differentially couples to distinct release pathways for IL-1beta in mouse macrophage. *J Immunol.* 2008;180(11):7147-7157.
23. Parzych K, Zetterqvist AV, Wright WR, Kirkby NS, Mitchell JA, Paul-Clark MJ. Differential role of pannexin-1/ATP/P2X(7) axis in IL-1 $\beta$  release by human monocytes. *FASEB J.* 2017;31(6):2439-2445.
24. Szabó C, Scott GS, Virág L, et al. Suppression of macrophage inflammatory protein (MIP)-1alpha production and collagen-induced arthritis by adenosine receptor agonists. *Br J Pharmacol.* 1998;125(2):379-387.
25. McWhinney CD, Dudley MW, Bowlin TL, et al. Activation of adenosine A3 receptors on macrophages inhibits tumor necrosis factor-alpha. *Eur J Pharmacol.* 1996;310(2-3):209-216.
26. Eltzschig HK, Thompson LF, Karhausen J, et al. Endogenous adenosine produced during hypoxia attenuates neutrophil accumulation: coordination by extracellular nucleotide metabolism. *Blood.* 2004;104(13):3986-3992.
27. Yago T, Tsukamoto H, Liu Z, Wang Y, Thompson LF, McEver RP. Multi-inhibitory effects of A2A adenosine receptor signaling on neutrophil adhesion under flow. *J Immunol.* 2015;195(8):3880-3889.
28. Frasson AP, Menezes CB, Goelzer GK, Gnoatto SCB, Garcia SC, Tasca T. Adenosine reduces reactive oxygen species and interleukin-8 production by *Trichomonas vaginalis*-stimulated neutrophils. *Purinergic Signal.* 2017;13(4):569-577.
29. Sun WC, Moore JN, Hurley DJ, Vandenplas ML, Murray TF. Effects of stimulation of adenosine A2A receptors on lipopolysaccharide-induced production of reactive oxygen species by equine neutrophils. *Am J Vet Res.* 2007;68(6):649-656.
30. Lappas CM, Rieger JM, Linden J. A2A adenosine receptor induction inhibits IFN-gamma production in murine CD4+ T cells. *J Immunol.* 2005;174(2):1073-1080.
31. Csóka B, Himer L, Selmeczy Z, et al. Adenosine A2A receptor activation inhibits T helper 1 and T helper 2 cell development and effector function. *FASEB J.* 2008;22(10):3491-3499.
32. Le Vraux V, Chen YL, Masson I, et al. Inhibition of human monocyte TNF production by adenosine receptor agonists. *Life Sci.* 1993;52(24):1917-1924.
33. Haskó G, Szabó C, Németh ZH, Kvetan V, Pastores SM, Vizi ES. Adenosine receptor agonists differentially regulate IL-10, TNF-alpha, and nitric oxide production in RAW 264.7 macrophages and in endotoxemic mice. *J Immunol.* 1996;157(10):4634-4640.
34. Silverman MH, Strand V, Markovits D, et al. Clinical evidence for utilization of the A3 adenosine receptor as a target to treat rheumatoid arthritis: data from a phase II clinical trial. *J Rheumatol.* 2008;35(1):41-48.
35. Fishman P, Cohen S. The A3 adenosine receptor (A3AR): therapeutic target and predictive biological marker in rheumatoid arthritis. *Clin Rheumatol.* 2016;35(9):2359-2362.
36. Milne GR, Palmer TM. Anti-inflammatory and immunosuppressive effects of the A2A adenosine receptor. *ScientificWorldJournal.* 2011;11:320-339.
37. Jacobson KA, Tosh DK, Jain S, Gao ZG. Historical and current adenosine receptor agonists in preclinical and clinical development. *Front Cell Neurosci.* 2019;13:124.
38. Flögel U, Burghoff S, van Lent PL, et al. Selective activation of adenosine A2A receptors on immune cells by a CD73-dependent prodrug suppresses joint inflammation in experimental rheumatoid arthritis. *Sci Transl Med.* 2012;4(146):146ra108.
39. Pulte ED, Broekman MJ, Olson KE, et al. CD39/NTPDase-1 activity and expression in normal leukocytes. *Thromb Res.* 2007;121(3):309-317.
40. Silva-Vilches C, Ring S, Mahnke K. ATP and its metabolite adenosine as regulators of dendritic cell activity. *Front Immunol.* 2018;9:2581.
41. Saze Z, Schuler PJ, Hong CS, Cheng D, Jackson EK, Whiteside TL. Adenosine production by human B cells and B cell-mediated suppression of activated T cells. *Blood.* 2013;122(1):9-18.
42. Gourdin N, Bossennec M, Rodriguez C, et al. Autocrine adenosine regulates tumor polyfunctional CD73(+)/CD4(+) effector T cells devoid of immune checkpoints. *Can Res.* 2018;78(13):3604-3618.
43. Yu N, Li X, Song W, et al. CD4(+)/CD25 (+)/CD127 (low/-) T cells: a more specific Treg population in human peripheral blood. *Inflammation.* 2012;35(6):1773-1780.
44. Thomson LF, Ruedi JM, Glass A, et al. Production and characterization of monoclonal antibodies to the glycosyl phosphatidylinositol-anchored lymphocyte differentiation antigen ecto-5'-nucleotidase (CD73). *Tissue Antigens.* 1990;35(1):9-19.
45. Quarona V, Ferri V, Chillemi A, et al. Unraveling the contribution of ectoenzymes to myeloma life and survival in the bone marrow niche. *Ann N Y Acad Sci.* 2015;1335:10-22.
46. Ohta M, Toyama K, Gutterman DD, et al. Ecto-5'-nucleotidase, CD73, is an endothelium-derived hyperpolarizing factor synthase. *Arterioscler Thromb Vasc Biol.* 2013;33(3):629-636.
47. Schuler PJ, Saze Z, Hong CS, et al. Human CD4+ CD39+ regulatory T cells produce adenosine upon co-expression of surface CD73 or contact with CD73+ exosomes or CD73+ cells. *Clin Exp Immunol.* 2014;177(2):531-543.
48. Botta Gordon-Smith S, Ursu S, Eaton S, Moncrieffe H, Wedderburn LR. Correlation of low CD73 expression on synovial lymphocytes with reduced adenosine generation and higher disease severity in juvenile idiopathic arthritis. *Arthritis Rheumatol.* 2015;67(2):545-554.
49. Yan K, Xu W, Huang Y, et al. Methotrexate restores the function of peripheral blood regulatory T cells in psoriasis vulgaris via the CD73/AMPK/mTOR pathway. *Br J Dermatol.* 2018;179(4):896-905.
50. Akhtari M, Zargar SJ, Mahmoudi M, Vojdani M, Rezaeimanesh A, Jamshidi A. Ankylosing spondylitis monocyte-derived macrophages express increased level of A2A adenosine receptor and decreased level of ectonucleoside triphosphate diphosphohydrolase-1 (CD39), A1 and A2B adenosine receptors. *Clin Rheumatol.* 2018;37(6):1589-1595.
51. Walscheid K, Neekamp L, Heiligenhaus A, et al. Peripheral blood monocytes reveal an activated phenotype in pediatric uveitis. *Clin Immunol.* 2018;190:84-88.
52. de Lourdes M-G, García-Rocha R, Morales-Ramírez O, et al. Mesenchymal stromal cells derived from cervical cancer produce high amounts of adenosine to suppress cytotoxic T lymphocyte functions. *J Transl Med.* 2016;14(1):302.

53. Jiang T, Xu X, Qiao M, et al. Comprehensive evaluation of NT5E/CD73 expression and its prognostic significance in distinct types of cancers. *BMC Cancer*. 2018;18(1):267.
54. Cai X-Y, Ni X-C, Yi Y, et al. Overexpression of CD39 in hepatocellular carcinoma is an independent indicator of poor outcome after radical resection. *Medicine*. 2016;95(40):e4989.
55. Cai XY, Wang XF, Li J, et al. High expression of CD39 in gastric cancer reduces patient outcome following radical resection. *Oncol Lett*. 2016;12(5):4080-4086.
56. Antonioli L, Fornai M, Blandizzi C, Pacher P, Hasko G. Adenosine signaling and the immune system: when a lot could be too much. *Immunol Lett*. 2019;205:9-15.
57. Stagg J, Divisekera U, McLaughlin N, et al. Anti-CD73 antibody therapy inhibits breast tumor growth and metastasis. *Proc Natl Acad Sci U S A*. 2010;107(4):1547-1552.
58. Figueiró F, Mendes FB, Corbelini PF, et al. A monastrol-derived compound, LaSOM 63, inhibits ecto-5-nucleotidase/CD73 activity and induces apoptotic cell death of glioma cell lines. *Anticancer Res*. 2014;34(4):1837-1842.
59. Häusler SF, Del Barrio IM, Diessner J, et al. Anti-CD39 and anti-CD73 antibodies A1 and 7G2 improve targeted therapy in ovarian cancer by blocking adenosine-dependent immune evasion. *Am J Transl Res*. 2014;6(2):129-139.
60. Young A, Ngiow SF, Barkauskas DS, et al. Co-inhibition of CD73 and A2AR adenosine signaling improves anti-tumor immune responses. *Cancer Cell*. 2016;30(3):391-403.
61. Allard D, Chrobak P, Allard B, Messaoudi N, Stagg J. Targeting the CD73-adenosine axis in immuno-oncology. *Immunol Lett*. 2019;205:31-39.
62. Lowenstein JM. Ammonia production in muscle and other tissues: the purine nucleotide cycle. *Physiol Rev*. 1972;52(2):382-414.
63. Dunkley CR, Manery JF, Dryden EE. The conversion of ATP to IMP by muscle surface enzymes. *J Cell Physiol*. 1966;68(3):241-247.
64. Manery JF, Riordan JR, Dryden EE. Characteristics of nucleotide-converting enzymes at muscle surfaces with special reference to ion sensitivity. *Can J Physiol Pharmacol*. 1968;46(3):537-547.
65. Pipoly GM, Nathans GR, Chang D, Deuel TF. Regulation of the interaction of purified human erythrocyte AMP deaminase and the human erythrocyte membrane. *J Clin Invest*. 1979;63(5):1066-1076.
66. Rao SN, Hara L, Askari A. Alkali cation-activated AMP deaminase of erythrocytes: some properties of the membrane-bound enzyme. *Biochem Biophys Acta*. 1968;151(3):651-654.
67. Atkinson DE. Regulation of enzyme activity. *Annu Rev Biochem*. 1966;35(1):85-124.
68. Chapman AG, Atkinson DE. Stabilization of adenylate energy charge by the adenylate deaminase reaction. *J Biol Chem*. 1973;248(23):8309-8312.
69. Johnson TA, Jinnah HA, Kamatani N. Shortage of cellular ATP as a cause of diseases and strategies to enhance ATP. *Front Pharmacol*. 2019;10:98.
70. Sabina RL, Swain JL, Olanow CW, et al. Myoadenylate deaminase deficiency. Functional and metabolic abnormalities associated with disruption of the purine nucleotide cycle. *J Clin Invest*. 1984;73(3):720-730.
71. Binkley PF, Auseon A, Cooke G. A polymorphism of the gene encoding AMPD1: clinical impact and proposed mechanisms in congestive heart failure. *Congest Heart Fail*. 2004;10(6):274-279; quiz 279-280.
72. Borkowski T, Slominska EM, Orlewska C, et al. Protection of mouse heart against hypoxic damage by AMP deaminase inhibition. *Nucleosides Nucleotides Nucleic Acids*. 2010;29(4-6):449-452.
73. Stewart SA, Dykxhoorn DM, Palliser D, et al. Lentivirus-delivered stable gene silencing by RNAi in primary cells. *RNA*. 2003;9(4):493-501.
74. Sarbassov DD, Guertin DA, Ali SM, Sabatini DM. Phosphorylation and regulation of Akt/PKB by the rictor-mTOR complex. *Science*. 2005;307(5712):1098-1101.
75. Rappsilber J, Ishihama Y, Mann M. Stop and go extraction tips for matrix-assisted laser desorption/ionization, nanoelectrospray, and LC/MS sample pretreatment in proteomics. *Anal Chem*. 2003;75(3):663-670.
76. Hughes CS, Moggridge S, Müller T, Sorensen PH, Morin GB, Krijgsveld J. Single-pot, solid-phase-enhanced sample preparation for proteomics experiments. *Nat Protoc*. 2019;14(1):68-85.
77. Perez-Riverol Y, Csordas A, Bai J, et al. The PRIDE database and related tools and resources in 2019: improving support for quantification data. *Nucleic Acids Res*. 2019;47(D1):D442-D450.
78. Cossarizza A, Chang HD, Radbruch A, et al. Guidelines for the use of flow cytometry and cell sorting in immunological studies. *Eur J Immunol*. 2017;47(10):1584-1797.
79. Ziegler-Heitbrock L, Ancuta P, Crowe S, et al. Nomenclature of monocytes and dendritic cells in blood. *Blood*. 2010;116(16):e74-e80.
80. Wu CH, Apweiler R, Bairoch A, et al. The Universal Protein Resource (UniProt): an expanding universe of protein information. *Nucleic Acids Res*. 2006;34(90001):D187-D191.
81. Sonnhammer EL, von Heijne G, Krogh A. A hidden Markov model for predicting transmembrane helices in protein sequences. *Proc Int Conf Intell Syst Mol Biol*. 1998;6:175-182.
82. Jones DT. Protein secondary structure prediction based on position-specific scoring matrices. *J Mol Biol*. 1999;292(2):195-202.
83. Gautier R, Douguet D, Antonny B, Drin G. HELIQUEST: a web server to screen sequences with specific alpha-helical properties. *Bioinformatics*. 2008;24(18):2101-2102.
84. Keller RC. Identification and in silico analysis of helical lipid binding regions in proteins belonging to the amphitropic protein family. *J Biosci*. 2014;39(5):771-783.
85. Sabina RL, Mahnke-Zizelman DK. Towards an understanding of the functional significance of N-terminal domain divergence in human AMP deaminase isoforms. *Pharmacol Ther*. 2000;87(2-3):279-283.
86. Thul PJ, Akesson L, Wiking M, et al. A subcellular map of the human proteome. *Science*. 2017;356(6340):eaal3321.
87. Uhlen M, Bandrowski A, Carr S, et al. A proposal for validation of antibodies. *Nat Methods*. 2016;13(10):823-827.
88. Eltzschig HK, Faigle M, Knapp S, et al. Endothelial catabolism of extracellular adenosine during hypoxia: the role of surface adenosine deaminase and CD26. *Blood*. 2006;108(5):1602-1610.
89. Stahn C, Buttgerit F. Genomic and nongenomic effects of glucocorticoids. *Nat Clin Pract Rheumatol*. 2008;4(10):525-533.
90. Strehl C, Ehlers L, Gaber T, Buttgerit F. Glucocorticoids—all-rounders tackling the versatile players of the immune system. *Front Immunol*. 2019;10:1744.
91. Baumann G, Rappaport G, Lemarchand-Béraud T, Felber JP. Free cortisol index: a rapid and simple estimation of free cortisol in human plasma. *J Clin Endocrinol Metab*. 1975;40(3):462-469.

92. Ballard PL. Delivery and transport of glucocorticoids to target cells. *Monogr Endocrinol.* 1979;12:25-48.
93. Peterson RE, Pierce CE, Wyngaarden JB, Bunim JJ, Brodie BB. The physiological disposition and metabolic fate of cortisone in man. *J Clin Investig.* 1957;36(9):1301-1312.
94. Webel ML, Ritts RE Jr, Taswell HF, Danadio JV Jr, Woods JE. Cellular immunity after intravenous administration of methylprednisolone. *J Lab Clin Med.* 1974;83(3):383-392.
95. Montesinos MC, Takedachi M, Thompson LF, Wilder TF, Fernandez P, Cronstein BN. The antiinflammatory mechanism of methotrexate depends on extracellular conversion of adenine nucleotides to adenosine by ecto-5'-nucleotidase: findings in a study of ecto-5'-nucleotidase gene-deficient mice. *Arthritis Rheum.* 2007;56(5):1440-1445.
96. Bossennec M, Rodriguez C, Hubert M, et al. Methotrexate restores CD73 expression on Th1.17 in rheumatoid arthritis and psoriatic arthritis patients and may contribute to its anti-inflammatory effect through adp production. *J Clin Med.* 2019;8(11):1859.
97. Figueiro F, de Oliveira CP, Bergamin LS, et al. Methotrexate up-regulates ecto-5'-nucleotidase/CD73 and reduces the frequency of T lymphocytes in the glioblastoma microenvironment. *Purinergic Signal.* 2016;12(2):303-312.
98. Kabisch S, Weigand T, Plischke H, Menninger H. Bioverfügbarkeit von Methotrexat (MTX) in unterschiedlichen Applikationsarten. *Aktuelle Rheumatol.* 2004;29(4):197-200.
99. Filippini A, Taffs RE, Sitkovsky MV. Extracellular ATP in T-lymphocyte activation: possible role in effector functions. *Proc Natl Acad Sci U S A.* 1990;87(21):8267-8271.
100. Burnstock G, Boeynaems JM. Purinergic signalling and immune cells. *Purinergic Signal.* 2014;10(4):529-564.
101. Linden J, Koch-Nolte F, Dahl G. Purine release, metabolism, and signaling in the inflammatory response. *Annu Rev Immunol.* 2019;37:325-347.
102. Gorini S, Gatta L, Pontecorvo L, Vitiello L, la Sala A. Regulation of innate immunity by extracellular nucleotides. *Am J Blood Res.* 2013;3(1):14-28.
103. Zetterström T, Vernet L, Ungerstedt U, Tossman U, Jonzon B, Fredholm BB. Purine levels in the intact rat brain. Studies with an implanted perfused hollow fibre. *Neurosci Lett.* 1982;29(2):111-115.
104. Hagberg H, Andersson P, Lacarewicz J, Jacobson I, Butcher S, Sandberg M. Extracellular adenosine, inosine, hypoxanthine, and xanthine in relation to tissue nucleotides and purines in rat striatum during transient ischemia. *J Neurochem.* 1987;49(1):227-231.
105. Kékesi V, Zima E, Barát E, et al. Pericardial concentrations of adenosine, inosine and hypoxanthine in an experimental canine model of spastic ischaemia. *Clin Sci.* 2002;103(Suppl 48):198s-201s.
106. Blay J, White TD, Hoskin DW. The extracellular fluid of solid carcinomas contains immunosuppressive concentrations of adenosine. *Can Res.* 1997;57(13):2602-2605.
107. Traut TW. Physiological concentrations of purines and pyrimidines. *Mol Cell Biochem.* 1994;140(1):1-22.
108. Linden J. Molecular approach to adenosine receptors: receptor-mediated mechanisms of tissue protection. *Annu Rev Pharmacol Toxicol.* 2001;41:775-787.
109. Marton A, Pacher P, Murthy KG, Németh ZH, Haskó G, Szabó C. Anti-inflammatory effects of inosine in human monocytes, neutrophils and epithelial cells in vitro. *Int J Mol Med.* 2001;8(6):617-621.
110. Welihinda AA, Kaur M, Greene K, Zhai Y, Amento EP. The adenosine metabolite inosine is a functional agonist of the adenosine A2A receptor with a unique signaling bias. *Cell Signal.* 2016;28(6):552-560.
111. Chen J, Chaurio RA, Maueröder C, et al. Inosine released from dying or dead cells stimulates cell proliferation via adenosine receptors. *Front Immunol.* 2017;8:504.
112. Smith TM, Kirley TL. Cloning, sequencing, and expression of a human brain ecto-apyrase related to both the ecto-ATPases and CD39 ecto-apyrases1. *Biochem Biophys Acta.* 1998;1386(1):65-78.
113. Klemens MR, Sherman WR, Holmberg NJ, Ruedi JM, Low MG, Thompson LF. Characterization of soluble vs membrane-bound human placental 5'-nucleotidase. *Biochem Biophys Res Comm.* 1990;172(3):1371-1377.
114. Weil-Malherbe H. The subcellular distribution of rat brain adenylyate deaminase and its association with neurostenin. *J Neurochem.* 1975;24(4):801-803.
115. Cuenda A, Henao F, Nogues M, Gutiérrez-Merino C. Quantification and removal of glycogen phosphorylase and other enzymes associated with sarcoplasmic reticulum membrane preparations. *Biochem Biophys Acta.* 1994;1194(1):35-43.
116. Sims B, Mahnke-Zizelman DK, Profit AA, Prestwich GD, Sabina RL, Theibert AB. Regulation of AMP deaminase by phosphoinositides. *J Biol Chem.* 1999;274(36):25701-25707.
117. Burn P. Amphitropic proteins: a new class of membrane proteins. *Trends Biochem Sci.* 1988;13(3):79-83.
118. Johnson JE, Cornell RB. Amphitropic proteins: regulation by reversible membrane interactions (review). *Mol Membr Biol.* 1999;16(3):217-235.
119. Halskau Ø, Muga A, Martínez A. Linking new paradigms in protein chemistry to reversible membrane-protein interactions. *Curr Protein Pept Sci.* 2009;10(4):339-359.
120. Sun X, Cárdenas A, Wu Y, Enyoji K, Robson SC. Vascular stasis, intestinal hemorrhage, and heightened vascular permeability complicate acute portal hypertension in cd39-null mice. *Am J Physiol Gastrointest Liver Physiol.* 2009;297(2):G306-G311.
121. Finn JD, Snoek S, van Ittersum J, et al. A8.12 AAV mediated expression of CD39 and CD73 is effective in reducing inflammation in the air pouch synovial inflammation model. *Ann Rheum Dis.* 2015;74(Suppl 1):A86.
122. Endo W, Arito M, Sato T, et al. Effects of sulfasalazine and tofacitinib on the protein profile of articular chondrocytes. *Mod Rheumatol.* 2014;24(5):844-850.
123. Luo Y, Zeng B, Zeng L, et al. Gut microbiota regulates mouse behaviors through glucocorticoid receptor pathway genes in the hippocampus. *Transl Psychiatry.* 2018;8(1):187.
124. Rouillard AD, Gunderson GW, Fernandez NF, et al. The harmonizome: a collection of processed datasets gathered to serve and mine knowledge about genes and proteins. *Database.* 2016;2016:baw100.
125. Lu Y, Cheng L, Li F, et al. The abnormal function of CD39(+) regulatory T cells could be corrected by high-dose dexamethasone in patients with primary immune thrombocytopenia. *Ann Hematol.* 2019;98(8):1845-1854.
126. Bavaresco L, Bernardi A, Braganhol E, Wink MR, Battastini AM. Dexamethasone inhibits proliferation and stimulates ecto-5'-nucleotidase/CD73 activity in C6 rat glioma cell line. *J Neurooncol.* 2007;84(1):1-8.

127. Sales-Campos H, de Souza PR, Basso PJ, et al. Amelioration of experimental colitis after short-term therapy with glucocorticoid and its relationship to the induction of different regulatory markers. *Immunology*. 2017;150(1):115-126.
128. Muls NG, Dang HA, Sindic CJ, van Pesch V. Regulation of Treg-associated CD39 in multiple sclerosis and effects of corticotherapy during relapse. *Mult Scler*. 2015;21(12):1533-1545.
129. Chan ES, Cronstein BN. Methotrexate—how does it really work? *Nature reviews. Rheumatology*. 2010;6(3):175-178.
130. Bedoui Y, Guillot X, Sélambarom J, et al. Methotrexate an old drug with new tricks. *Int J Mol Sci*. 2019;20(20):5023.
131. Wessels JA, Kooloos WM, De Jonge R, et al. Relationship between genetic variants in the adenosine pathway and outcome of methotrexate treatment in patients with recent-onset rheumatoid arthritis. *Arthritis Rheum*. 2006;54(9):2830-2839.
132. Peres RS, Liew FY, Talbot J, et al. Low expression of CD39 on regulatory T cells as a biomarker for resistance to methotrexate therapy in rheumatoid arthritis. *Proc Natl Acad Sci U S A*. 2015;112(8):2509-2514.
133. Taylor PC, Balsa Criado A, Mongey AB, Avouac J, Marotte H, Mueller RB. How to get the most from methotrexate (MTX) treatment for your rheumatoid arthritis patient?—MTX in the treat-to-target strategy. *J Clin Med*. 2019;8(4):515.
134. Herrath J, Chemin K, Albrecht I, Catrina AI, Malmström V. Surface expression of CD39 identifies an enriched Treg-cell subset in the rheumatic joint, which does not suppress IL-17A secretion. *Eur J Immunol*. 2014;44(10):2979-2989.
135. Akizu N, Cantagrel V, Schroth J, et al. AMPD2 regulates GTP synthesis and is mutated in a potentially treatable neurodegenerative brainstem disorder. *Cell*. 2013;154(3):505-517.
136. Ogasawara N, Goto H, Yamada Y, et al. Deficiency of AMP deaminase in erythrocytes. *Hum Genet*. 1987;75(1):15-18.
137. Dornand J, Clofent G, Bonnafous JC, Favero J, Mani JC. Purine metabolizing enzymes of lymphocyte cell populations: correlation between AMP-deaminase activity and dATP accumulation in murine lymphocytes. *Proc Soc Exp Biol Med*. 1985;179(4):448-455.
138. Guo G, Wang H, Shi X, et al. NovelmiRNA-25 inhibits AMPD2 in peripheral blood mononuclear cells of patients with systemic lupus erythematosus and represents a promising novel biomarker. *J Transl Med*. 2018;16(1):370.
139. Welihinda AA, Kaur M, Raveendran KS, Amento EP. Enhancement of inosine-mediated A(2A)R signaling through positive allosteric modulation. *Cell Signal*. 2018;42:227-235.
140. da Rocha LF, da Silva MD, de Almeida CD, Santos AR. Anti-inflammatory effects of purine nucleosides, adenosine and inosine, in a mouse model of pleurisy: evidence for the role of adenosine A2 receptors. *Purinergic Signal*. 2012;8(4):693-704.
141. Guinzberg R, Cortés D, Díaz-Cruz A, Riveros-Rosas H, Villalobos-Molina R, Piña E. Inosine released after hypoxia activates hepatic glucose liberation through A3 adenosine receptors. *Am J Physiol Endocrinol Metab*. 2006;290(5):E940-E951.
142. Shinohara Y, Tsukimoto M. Guanine and inosine nucleotides/nucleosides suppress murine T cell activation. *Biochem Biophys Res Comm*. 2018;498(4):764-768.
143. Haskó G, Kuhel DG, Németh ZH, et al. Inosine inhibits inflammatory cytokine production by a posttranscriptional mechanism and protects against endotoxin-induced shock. *J Immunol*. 2000;164(2):1013-1019.
144. Qiu FH, Wada K, Stahl GL, Serhan CN. IMP and AMP deaminase in reperfusion injury down-regulates neutrophil recruitment. *Proc Natl Acad Sci U S A*. 2000;97(8):4267-4272.
145. Möser GH, Schrader J, Deussen A. Turnover of adenosine in plasma of human and dog blood. *Am J Physiol*. 1989;256(4 Pt 1):C799-C806.
146. Viegas TX, Omura GA, Stoltz RR, Kisicki J. Pharmacokinetics and pharmacodynamics of peldesine (BCX-34), a purine nucleoside phosphorylase inhibitor, following single and multiple oral doses in healthy volunteers. *J Clin Pharmacol*. 2000;40(4):410-420.

## SUPPORTING INFORMATION

Additional Supporting Information may be found online in the Supporting Information section.

**How to cite this article:** Ehlers L, Kuppe A, Damerau A, et al. Surface AMP deaminase 2 as a novel regulator modifying extracellular adenine nucleotide metabolism. *The FASEB Journal*. 2021;35:e21684. <https://doi.org/10.1096/fj.202002658RR>

## APPENDIX

### Monocytic expression of CD73 is dependent on cell culture conditions

Besides our main findings, we observed a strong increase in monocytic CD73 expression during cell culture. Interestingly, this effect was only observed in cultures containing human serum while CD73 expression remained low in monocytes cultured in medium supplemented with FCS (Appendix Figure A1). As a marked expression of CD73 has been described as a characteristic feature of M2 macrophages, we hypothesised that the presence of human serum promoted monocyte adhesion and thereby differentiation towards a macrophage phenotype.<sup>1-3</sup> As a side note, CD73 was also considerably upregulated in THP-1 cells incubated with PMA. While this activation was likewise associated with cell adhesion even in the absence of human serum, the cells remained in suspension upon stimulation with LPS and did not show an upregulation of CD73 under these conditions (Appendix Figure A2). The abundance of CD73 in macrophages as a tissue-resident cell type is consistent with the fact that adenosine as the product of this ectonucleotidase has a very short half-life in comparison with other purine metabolites.<sup>4,5</sup> Its action is therefore confined to its production site, which is in accordance with the low expression of CD73 in circulating monocytes.

## REFERENCES

1. Monguio-Tortajada M, Roura S, Galvez-Monton C, Franquesa M, Bayes-Genis A, Borrás FE. Mesenchymal stem cells induce expression of CD73 in human monocytes in vitro and in a swine model of myocardial infarction in vivo. *Front Immunol*. 2017;8:1577.



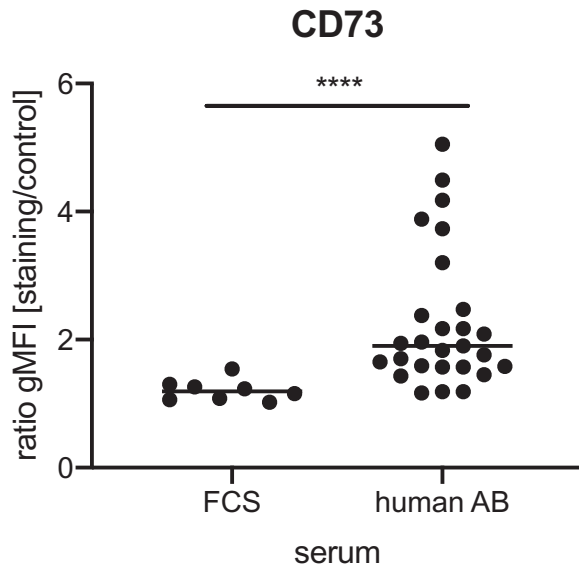


**FIGURE A1** PBMCs were co-cultured in RPMI supplemented with either FCS or human AB serum for 24 hours. Monocytic CD73 surface expression was determined by flow cytometry. Monocytes were gated according to Supplementary Figure S1E for analysis. Lines on scatter dot plot represent median. \*\*\*\* $P < .0001$ , Mann Whitney test.

- Ohradanova-Repic A, Machacek C, Charvet C, et al. Extracellular purine metabolism is the switchboard of immunosuppressive macrophages and a novel target to treat diseases with macrophage imbalances. *Front Immunol.* 2018;9:852.
- Zanin RF, Braganhol E, Bergamin LS, et al. Differential macrophage activation alters the expression profile of NTPDase and ecto-5'-nucleotidase. *PLoS One.* 2012;7(2):e31205.

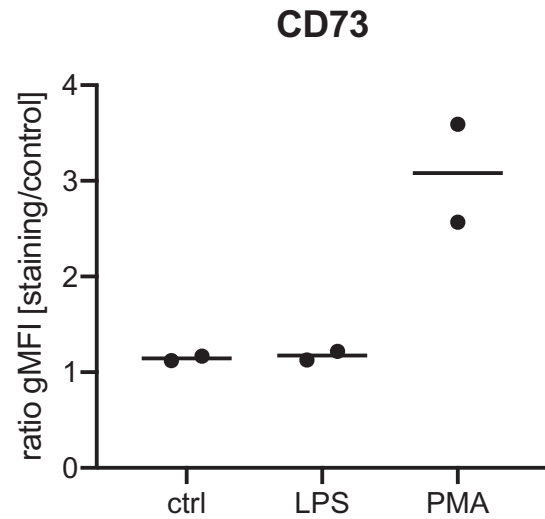


**FIGURE A2** Flow cytometric analysis of CD73 surface expression on THP-1 cells stimulated with 1  $\mu\text{g}/\text{mL}$  LPS or 10  $\text{ng}/\text{mL}$  PMA for 24 hours. Cells were gated according to Supplementary Figure S1F for analysis.

- Möser GH, Schrader J, Deussen A. Turnover of adenosine in plasma of human and dog blood. *Am J Physiol.* 1989 Apr;256(4 Pt 1):C799-C806.
- Viegas TX, Omura GA, Stoltz RR, Kisicki J. Pharmacokinetics and pharmacodynamics of peldesine (BCX-34), a purine nucleoside phosphorylase inhibitor, following single and multiple oral doses in healthy volunteers. *J Clin Pharmacol.* 2000 Apr;40(4):410-420.